AGU PUBLICATIONS

JGR

Journal of Geophysical Research: Oceans

RESEARCH ARTICLE

10.1002/2015JC010826

**Key Points:**
- Coastal eddies sustain biological production for several months in EBUS
- Eddy trapping and eddy pumping help to isolate and maintain ecosystem dynamics
- Coastal eddy dynamics drive a vertical decoupling of the ecosystem

**Correspondence to:**
F. Chenillat,
fchenillat@ucsd.edu

**Citation:**
Chenillat, F., P. J. S. Franks, P. Rivière, X. Capet, N. Grima, and B. Blanke (2015), Plankton dynamics in a cyclonic eddy in the Southern California Current System, *J. Geophys. Res. Oceans*, *120*, 5566–5588, doi:10.1002/2015JC010826.

Received 11 MAR 2015
Accepted 8 JUL 2015
Accepted article online 14 JUL 2015
Published online 14 AUG 2015



# Plankton dynamics in a cyclonic eddy in the Southern California Current System

**Fanny Chenillat[1], Peter J. S. Franks[1], Pascal Rivière[2], Xavier Capet[3], Nicolas Grima[4], and Bruno Blanke[4]**

[1]Integrative Oceanography Division, Scripps Institution of Oceanography, University of California, San Diego, La Jolla, California, USA, [2]Laboratoire des Sciences de l'Environnement Marin, UMR 6539 CNRS-UBO-IRD-Ifremer, Institut Universitaire Européen de la Mer (IUEM), Plouzané, France, [3]Laboratoire d'Océanographie et du Climat, CNRS-UPMC-IRD-MNHN, Institut Pierre Simon Laplace (IPSL), Paris, France, [4]Laboratoire de Physique des Océans, UMR 6523 CNRS-Ifremer-IRD-UBO, Université de Brest Occidentale, Brest, France

**Abstract** The California Current System is an eastern boundary upwelling system (EBUS) with high biological production along the coast. Oligotrophic offshore waters create cross-shore gradients of biological and physical properties, which are affected by intense mesoscale eddy activity. The influence of eddies on ecosystem dynamics in EBUS is still in debate. To elucidate the mechanisms that influence the dynamics of ecosystems trapped in eddies, and the relative contribution of horizontal and vertical advection in determining local production, we analyze a particular cyclonic eddy using Lagrangian particle-tracking analyses of numerical Eulerian. The eddy formed in a coastal upwelling system; coastal waters trapped in the eddy enabled it to leave the upwelling region with high concentrations of plankton and nutrients. The ecosystem was initially driven mainly by recycling of biological material. As the eddy moved offshore, production in its core was enhanced compared to eddy exterior waters through Ekman pumping of nitrate from below the euphotic zone; this Ekman pumping was particularly effective due to the shallow nitracline in the eddy compared to eddy exterior waters. Both eddy trapping and Ekman pumping helped to isolate and maintain the ecosystem productivity in the eddy core. This study shows the importance of cyclonic eddies for biological production in EBUS: they contribute both to the redistribution of the coastal upwelling ecosystem and are local regions of enhanced new production. Together, these processes impact cross-shore gradients of important biological properties.

## 1. Introduction

The California Current System (CCS) is an eastern boundary upwelling system (EBUS) characterized by upwelling of cold, salty, nutrient-rich water that supports high biological production along the coast. Low production in the oligotrophic offshore waters creates a strong cross-shore gradient controlled by both offshore Ekman transport and fluxes associated with intense mesoscale activity [*Capet et al.*, 2008; *Chaigneau et al.*, 2009, 2011; *Sangrà et al.*, 2009; *Colas et al.*, 2011]. This mesoscale activity, and in particular its role in controlling ecosystem dynamics, is the focus of the present study.

The effect of mesoscale turbulence on biogeochemical activity has been a subject of interest for several decades [e.g., *Gower et al.*, 1980; *Jenkins*, 1988; *Mcgillicuddy et al.*, 1998; *McGillicuddy and Johnson*, 1999; *McGillicuddy and Kosnyrev*, 2001; *Lévy*, 2008; *Klein and Lapeyre*, 2009]. Although the basic mechanisms through which mesoscale turbulence can act on oceanic tracers are well understood [*Bleck et al.*, 1988; *Gent and McWilliams*, 1990; *Lee et al.*, 1997], biogeochemical responses are complex due to the mixture of contrasting flow regimes, including coherent eddies, jets, filaments, and fronts. These various dynamical regimes have contrasting effects on biological and chemical fluxes [*Lapeyre and Klein*, 2006], which have their own inherent time and space scales of response.

To quantify bulk, regional-scale effects of mesoscale turbulence on biogeochemical tracers, comparisons are often made between eddy-resolving and noneddy-resolving models [e.g., *Lévy et al.*, 2001, 2012; *Capet et al.*, 2008; *Ivchenko et al.*, 2008; *Oschlies*, 2008; *Gruber et al.*, 2011]. In EBUS, such studies have shown that mesoscale turbulence *reduces* net primary production through two main mechanisms: the cross-shore transport associated with upwelling filaments and jets, and the vertical export of nutrients [*Gruber et al.*, 2011] and phytoplankton biomass [*Lathuilière et al.*, 2010].

In contrast to the regional-scale, bulk responses of many models, field experiments often focus on individual turbulent features, fronts, or vortices. In concert, new modeling approaches have been developed to identify and track particular turbulent features [*Chelton et al*., 2011a]. As individual entities, eddies appear to *enhance* biological activity compared to the waters exterior to the eddies, in both open-ocean regions [*Gower et al*., 1980; *Strass*, 1992; *Allen et al*., 1996; *Mcgillicuddy et al*., 1998; *McGillicuddy and Johnson*, 1999; *McGillicuddy and Kosnyrev*, 2001] and EBUS [*McGowan*, 1967; *Owen*, 1980; *Hayward and Mantyla*, 1990; *Thomas*, 1999; *Correa-Ramirez*, 2007].

Several mechanisms have been proposed to explain the enhanced biogeochemical activity associated with individual eddies in the open ocean. First, eddy cores are nonlinear, coherent features [*Chelton et al*., 2011b], that trap fluid parcels, nutrients, and biota and transport them hundreds of kilometers and over several months [*Flierl*, 1981; *Siegel et al*., 1999; *Early et al*., 2011; *Haury et al*., 1978; *The Ring Group*, 1981; *Woods*, 1988]. Furthermore, within the eddy core the vertical displacement of isopycnals during eddy formation through baroclinic instability [*Carton*, 2010], combined with locally enhanced vertical velocities can drive nutrient fluxes into/out of the euphotic zone [*Franks et al*., 1986; *Woods*, 1988; *Falkowski et al*., 1991; *McGillicuddy and Robinson*, 1997; *Oschlies and Garcon*, 1998; *Oschlies*, 2002; *McGillicuddy et al*., 2007]. One mechanism causing such vertical velocities is Ekman pumping, created through the curl of the local wind stress [*Yentsch and Phinney*, 1985; *Jenkins*, 1988; *Falkowski et al*., 1991; *McGillicuddy and Robinson*, 1997]. Within the cyclonic eddy, the deformations of the isopycnals move the nitracline upward. Ekman pumping can then act on this already-shoaled nitracline to further shoal it into the euphotic zone. Acting together, the deformations of the nitracline due to the cyclonic eddy and Ekman pumping may be an important mechanism controlling biological productivity and planktonic ecosystem structure in mesoscale features.

In EBUS, the high productivity associated with mesoscale eddies has been explained through the interaction of horizontal transport and vertical advection [*Crawford*, 2005; *Brzezinski and Washburn*, 2011; *Lehahn et al*., 2011; *Morales et al*., 2012], though their relative contributions are often difficult to quantify [*Lévy*, 2008]. In EBUS where eddies form nearshore, eddy productivity will depend on numerous factors, including the nutrient concentrations and planktonic community present in the eddy's source waters [*Bibby et al*., 2008; *Mahaffey et al*., 2008], the horizontal transport efficiency [*Brown et al*., 2008; *Lévy*, 2008; *Siegel et al*., 2011], and the local physical and biological dynamics of the eddy [*The Ring Group*, 1981; *Benitez-Nelson et al*., 2007; *Bibby et al*., 2008; *Almazán-Becerril et al*., 2012; *Stramma et al*., 2013].

The discrepancies among regional-scale and local-scale studies, i.e., the apparent reduction in primary production at the regional scale versus enhancement of primary production at the local scale, points to a lack of understanding of the ecological role of eddies in upwelling systems and their effects on ecosystem dynamics. Here we attempt to elucidate the mechanisms that influence the dynamics of ecosystems trapped in cyclonic eddies of EBUS, and the relative contributions of horizontal and vertical advection in determining biological production in the eddies.

To assess the influences of eddies on ecosystem dynamics, we focus on one particular eddy in the Southern CCS from a numerical experiment (detailed in section 2.1). The formation and kinematic evolution of a cyclonic eddy were quantified using Lagrangian particle-tracking analyses [*Blanke and Raynaud*, 1997; *Blanke et al*., 1999; *Chenillat et al*., 2015] (see Figure 1 and section 2.2). This eddy formed at the end of the summer from a coastal meander, through instabilities of the alongshore current. As it formed, the eddy trapped coastal material that created a core with $>$90% of its water of coastal origin. Subsequent waters wrapped around the eddy, forming concentric layers of different ages, with the oldest water at the core and the youngest at the eddy's edge. The outermost rings were composed of only $\sim$70% coastal waters. This eddy detached from the coast around January of the following year, and moved offshore until June. The eddy was a coherent structure during this time—its rotational fluid speed was greater that its translation speed—with weak horizontal exchange among the concentric rings (Figure 1b). The core of this cyclonic eddy retained coastal waters for $\sim$6 months and was in approximate solid-body rotation for $\sim$2 months (Figure 1c): the two particle pools closest to the eddy center had the same angular velocity $\omega$ [*Sangrà et al*., 2005]. These central particle pools were uncoupled from the waters at the edge of the eddy. The trapped coastal, nutrient-rich core water isolated the planktonic ecosystem from horizontal losses and apparently drove locally enhanced biological productivity for several months. In this study, we diagnose the dynamics leading to the local ecosystem response, and estimate the relative contributions of coastal and local inputs.

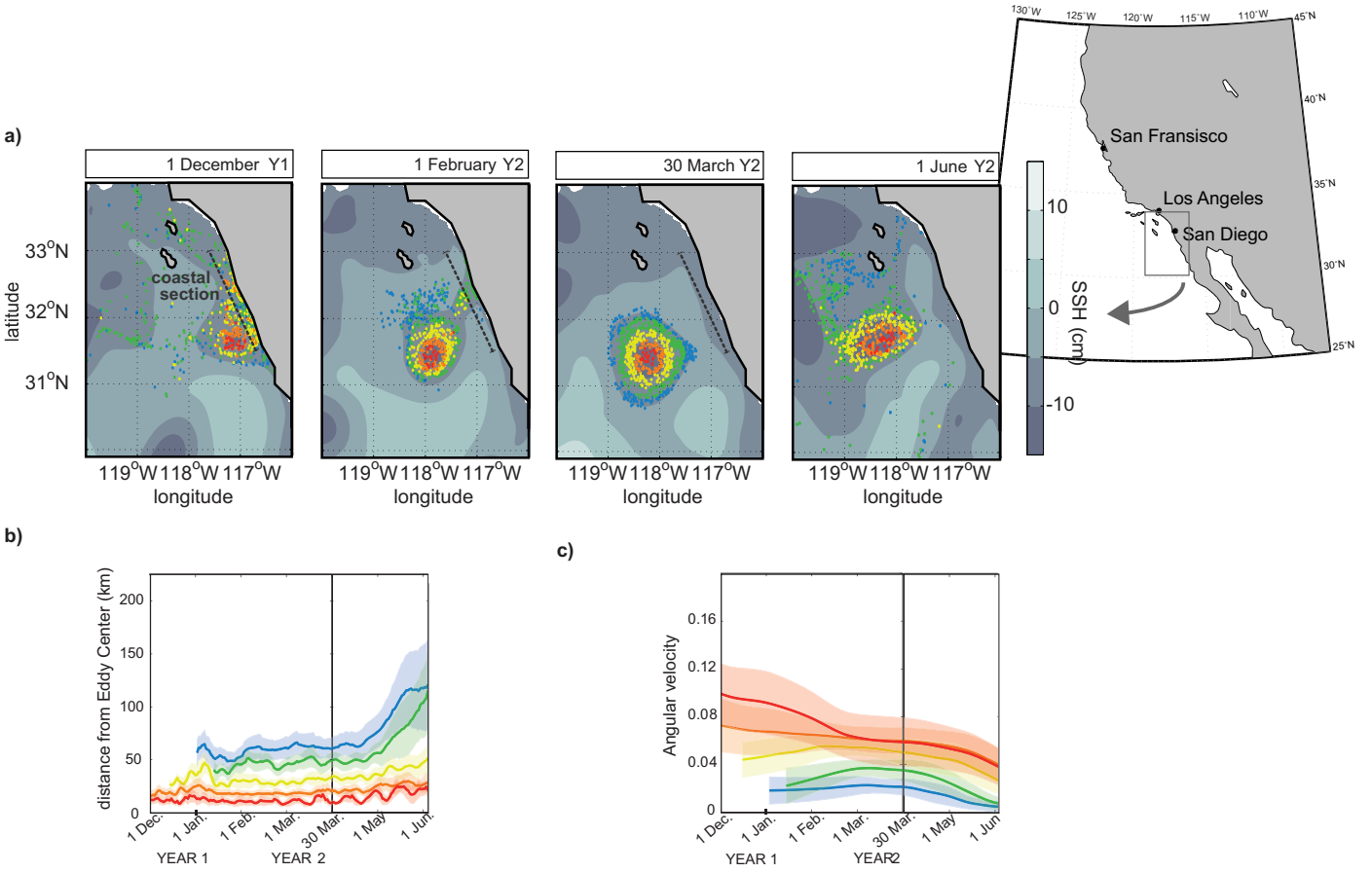


**Figure 1.** Kinematic of the cyclonic eddy in the Southern CCS. (a) Bimonthly daily mean modeled SSH (grey scale, in cm). On 30 March Y2, Lagrangian particles were initialized in the cyclonic eddy. Different pools were colored based on their initial position in the eddy and tracked backward (e.g., 1 December Y1 and 1 February Y2) and forward (e.g., 1 June Y2) in time using the Ariane Lagrangian module. Each dot corresponds to one particle. The color for each particle pool is used consistently with (b) and (c). The dashed line in in panels of Figure 1a indicates the coastal section through which particles passed before entering the eddy. Of the 1260 total particles in use, only the 843 particles that entered the eddy are shown in figure 1a. (b) and (c) Temporal evolution for each particle pool of the distance from the eddy center, and the corresponding angular velocity. The black lines at 30 March Y2 indicate the initial time (30 March Y2) since the eddy is followed backward or forward in time.

Here we describe and quantify the planktonic ecosystem dynamics in the eddy core, and compare them with waters outside the eddy (Figure 2). Section 2 describes the numerical models and the methodology used; section 3 presents an evaluation of our model to accurately reproduce biological fields; sections 4 and 5 describe the main patterns of the ecosystem in the eddy and the underlying biological-physical processes, respectively. Section 6 provides estimates of the relative contributions of horizontal transport of coastal material versus local vertical input to the ecosystem dynamics in the eddy. A synthesis of this work is given in section 7.

## 2. Numerical Models and Methodology

### 2.1. Physical-Biogeochemical Eulerian Model

Using a coupled physical-biogeochemical model, we investigate the effects of mesoscale dynamics on planktonic ecosystems in the Southern California Current System (SCCS), focusing on the dynamics within a single cyclonic eddy.

The physical model is the Regional Ocean Modeling System (ROMS), a three-dimensional, free-surface, hydrostatic, eddy-resolving primitive equation ocean model [*Shchepetkin and McWilliams*, 2005]. This model was configured with a 5 km resolution horizontal grid covering the entire west coast of the United States from the coast to 1000 km offshore and from southern Canada (50°N) to southern Baja California, Mexico (24°N) (as in *Capet et al.* [2008]), thus capturing the entire California Current System (CCS). The 32 vertical $\sigma$-coordinate levels, with higher resolution near the surface, resolve the upper ocean physical and ecosystem dynamics. The bathymetry is derived from etopo2 (http://www.ngdc.noaa.gov/mgg/global/etopo2.html) following the

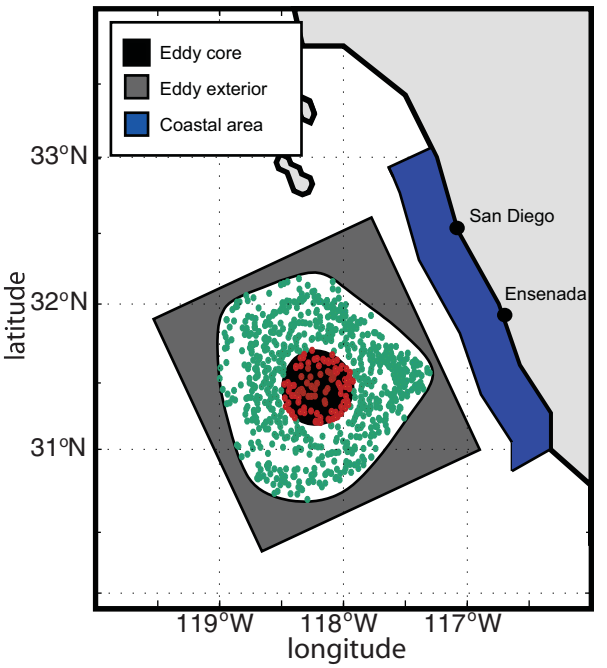


**Figure 2.** Schematic representation of the domains of interest: the eddy core (in black), the eddy exterior (in grey), and coastal area (in blue). This color code will be used throughout the paper. The dots represent the eddy-trapped particles from the Lagrangian experiment on 30 March Y2: the eddy core is depicted by the red particles that are in approximate solid-body rotation (Figure 1c); the green particles are the outermost particles that help to diagnose the edge of the eddy, and thus the eddy exterior area.

procedure of *Penven et al.* [2008]. The physical boundary conditions, initial conditions, and surface forcings used in this study are similar to *Capet et al.* [2008]: boundary conditions and surface forcings are climatological. Monthly averages from the Comprehensive Ocean-Atmosphere Data set (COADS) are used for surface fluxes, except for temperature which was obtained from Advanced Very High-Resolution Radiometer (AVHRR). The monthly climatology for the wind forcing is computed from QuikSCAT satellite scatterometer data for the period 2000–2008. Initial and open boundary conditions come from a monthly climatology computed from the Simple Ocean Data Assimilation (SODA) model [*Carton and Giese*, 2008].

The biogeochemical model is the lower trophic level ecosystem model NEMURO (North Pacific Ecosystem Model for Understanding Regional Oceanography) [*Kishi et al.*, 2007], with two phytoplankton size classes (small, and large, denoted as *PS* and *PL*, respectively), and three zooplankton size classes (small, large, and predator, denoted as *ZS*, *ZL*, and *ZP*, respectively). This model is based on nitrogen and silicon biogeochemical cycles. Nitrogen is found in all biological compartments, while silica transits exclusively through *PL*, which represents diatom-like phytoplankton, and to its consumers, *ZL* and *ZP*. The nutrient pool consists of nitrate ($NO_3^-$), ammonium ($NH_4^+$), and silicic acid ($Si(OH)_4$). The detritic pool includes particulate and dissolved organic nitrogen (*PON* and *DON*, respectively) and particulate silica (*Opal*). The evolution of these 11 state variables—or tracer concentrations—can be described by the advection-diffusion equation:

$$\frac{\partial C}{\partial t} + \vec{u} \cdot \nabla C = Diffusion + Sources - Sinks$$

where $C$ is the tracer concentration, the $\partial/\partial t$ operator is the local rate of change of the tracer, $\vec{u}$ is the local mean velocity field, and $\nabla C$ is the spatial gradient of $C$. The *Sources* and *Sinks* terms represent the biological gains and losses driven by biological fluxes, described in Table 1. The ratio *Si:N* is fixed at 2 in this model, in accordance with observations in the CCS from the Levitus World Ocean Atlas [*Garcia et al.*, 2006]. NEMURO was originally configured for the North Pacific Ocean and has been widely used in the CCS [*Rose et al.*, 2007; *Wainwright et al.*, 2003; *Li et al.*, 2010; *Chenillat et al.*, 2012, 2013]. The parameterization of NEMURO is the same as in *Chenillat et al.* [2013]. Biological initial conditions and boundary conditions were based on OFES (Ocean general circulation model For the Earth Simulator [*Masumoto et al.*, 2004; *Sasaki et al.*, 2004, 2006]) as in *Chenillat et al.* [2013].

The model was spun up for 40 years (30 for the physical model alone, and 10 for the coupled biological-physical model); daily averages of all the physical and biological variables were archived over the final 2 years, denoted Y1 and Y2, respectively. Physical and biological fluxes are calculated online during the model runs. The physical and biological data are then averaged over a day, and archived for Y1 and Y2.

### 2.2. Lagrangian Model and Domain Definitions

To highlight the biological roles of the cyclonic eddy described in Figure 1a, and to understand its ability to maintain high planktonic productivity for several months (see section 4), we compared the biological

**Table 1.** Description of Biological Sources and Sinks (See Equation (1)) for the Four Main Pools: Phytoplankton, Zooplankton, Nutrients, and Detritus [See *Kishi et al*., 2007 for Details]

| | *Sources* | *Sinks* |
|---|---|---|
| Nutrient ($NO_3^-$, $NH_4^+$, *Si(OH)4*) | (1) Recycling (called nitrification for $NO_3^-$), and (2) excretion (only for $NH_4^+$) | (1) Uptake for primary production (new and regenerated production), and (2) nitrification (only for $NH_4^+$) |
| Phytoplankton (*PS, PL*) | Growth by (1) new and (2) regenerated production | (1) Grazing by zooplankton, and (2) natural mortality |
| Zooplankton (*ZS, ZL, ZP*) | (1) Grazing on phytoplankton, and (2) predation on smaller zooplankton | (1) Predation by larger zooplankton, (2) natural mortality, (3) excretion, and (4) egestion |
| Detritus (*PON*, *DON*, *Opal*) | (1) Natural mortality, (2) egestion (concerned particulate pools only i.e., *PON* and *Opal*), and (3) recycling (only for DON) | (1) Recycling and (2) vertical sinking (concerned particulate pools only i.e., *PON* and *Opal*) |

dynamics in the eddy core with two noneddy regions: a coastal section in the coastal upwelling region where the eddy originated, and the waters surrounding the eddy ("eddy exterior") as it moved offshore (Figure 2). Comparisons of the eddy core to the coastal region will help quantify the ability of the eddy core to trap coastal biological material, while analyses of the eddy exterior waters will allow us to test the hypothesis that the biological patterns in the eddy core result from local eddy-influenced dynamics.

The horizontal extent of the eddy core was defined using the results of the Lagrangian experiments (Figure 1a). These experiments consisted of seeding the coastline (from 29.2°N to 33.1°N, and from the surface to a maximum of 200 m depth) each month with 210 particles, from September Y1 to February Y2 [*Chenillat et al*., 2015]. These particles were tracked forward in time until 30 March Y2, when the coastal eddy had moved offshore. The eddy core was defined by the area covered by the particles in approximate solid-body rotation (Figure 1c).

The inner edge of the region surrounding the eddy (the eddy exterior) was also defined using the Lagrangian experiments: it was the average *SSH* value of the outermost particles of the eddy in the Lagrangian experiments. The eddy exterior area was a square box with 100 km long sides. The sides followed the general orientation of the coastline (cross-shore/along-shore), and the box was centered on the eddy center, defined as the minimum of *SSH*. The areas of the regions defined for the eddy core and eddy exterior do not change a great deal (5000 $km^2 \pm 500$ $km^2$ (mean $\pm$ standard deviation) from 1 November Y1 to 1 June Y2) before the decay of the eddy (Figure 1a).

The coastal box was bounded horizontally by latitudes 31°N and 33°N, the coastline, and a line parallel to the coast positioned 30 km offshore. This domain represents the coastal upwelling region and contains the 135 km long coastal control section (Figure 1a) through which all particles of the Lagrangian experiment transited before being incorporated into the eddy.

The analyses spanned the period 1 November Y1 to 1 June Y2, i.e., from the formation of the eddy core to the beginning of its dissipation by the merging of the outermost particles with another mesoscale structure (Figure 1a).

### 2.3. Diagnoses

#### 2.3.1. Euphotic Depth

Some subsequent analyses are depth-integrated over the euphotic zone of the given region. The euphotic depth ($z_{euph}$) was computed each day of the run based on the diffuse attenuation coefficient of seawater and the attenuation due to the total phytoplankton concentration (sum of *PS* and *PL*). For each subdomain, a daily spatially averaged $z_{euph}$ was calculated from 1 November Y1 to 1 June Y2. This calculation gave the same $z_{euph}$ as that calculated using chlorophyll from the model.

#### 2.3.2. Biological Concentrations, Fluxes, and Specific Rates

The structure and functioning of the ecosystem were analyzed using the modeled biological concentrations $C$ (in mmol N $m^{-3}$) and biological fluxes $F$ (in mmol N $m^{-3}$ $d^{-1}$). The biological fluxes represent the exchanges of nitrogen and silica among the compartments of the biogeochemical model, and losses of particulate matter from the euphotic zone by vertical sinking. Both $C$ and $F$ were horizontally averaged over each region to find their average vertical structure as a function of time, and are denoted $\bar{C}$ and $\bar{F}$,

respectively. The vertical integration of $\bar{C}$ and $\bar{F}$ over $z_{euph}$, noted $\bar{C}_{int}$ and $\bar{F}_{int}$, gives their values averaged over the entire subdomain. The standard deviations within each subdomain provide a measure of variability and uncertainty. Specific rates (in $d^{-1}$), i.e., remineralization, growth, and grazing rates, were computed from appropriate ratios of $\bar{F}_{int}/\bar{C}_{int}$. The control areas and the control volumes changed little over time, and this has only a small impact on the estimation of $\bar{F}$, $\bar{C}$, $\bar{F}$ and $\bar{C}$.

#### 2.3.3. Advective Fluxes

The advective fluxes of a tracer represent the transport of this tracer by the flow. In general, an advective flux (in mmol N $m^{-2}$ $d^{-1}$) is quantified as:

$$Adv_C = \overline{C \times velocity}$$

with $C$ the biological concentration and *velocity* the vertical ($w$) or horizontal ($u$,$v$) component of the velocity. Both $C$ and *velocity* outputs were averaged daily. Here we define the advective fluxes of biological properties through different surfaces. The vertical advective flux $vAdv_C$ was calculated using the vertical velocity at the mean euphotic depth of the region, and was limited horizontally by the area of the region. The horizontal advective flux $hAdv_C$ was calculated using the horizontal velocity through the horizontal boundaries of the region, extending from the surface down to the mean euphotic depth of the region. Again, the control volume changed little over time, and the effect on the fluxes was limited.

#### 2.3.4. Ekman Pumping

The linear Ekman pumping, $W_E$, (in m $d^{-1}$), is the vertical velocity driven by the curl of the local surface wind stress:

$$W_E = \nabla \times \tau / \rho f$$

with $\nabla \times \tau$ the wind stress curl, $\rho$ the surface density of sea water, and $f$ the Coriolis frequency. Nonlinear Ekman pumping takes place at the submesoscale from eddy/wind interactions [e.g., *Thomas and Rhines*, 2002; *Thomas*, 2005; *Mahadevan et al*., 2008] and is neglected here because it is not well resolved by the 5 km resolution used for the model. $W_E$ was computed daily over the whole domain, and then averaged horizontally over each region.

## 3. Model Assessment

The coupled ROMS-NEMURO model was used successfully in a 15 km horizontal resolution configuration in *Chenillat et al*. [2013], and was found complex enough to realistically reproduce the cross-shore gradients of the regional upwelling system. In the present study, we use 5 km horizontal resolution to better resolve the mesoscale dynamics [*Capet et al*., 2008; *Kurian et al*., 2011].

This high-resolution coupled model produces lower coastal primary production compared to the coarser-resolution configuration [*Chenillat et al*., 2013]. This lower production is a direct consequence of increasing the resolution which creates (i) higher local vertical velocities combined with reduced average vertical velocities in most areas, and (ii) increased offshore mesoscale export from the coast [*Lathuilière et al*., 2010; *Gruber et al*., 2011]. The main biological properties of this model, averaged over the last 5 years of the coupled physical-biological spin-up, compare well with in situ annual climatological observations from CalCOFI (California Cooperative Oceanic Fisheries Investigations), averaged over 1949–2000 (Figure 3). Along the cross-shore section of line 90 of CalCOFI (from 33.4°N 117.9°W at the coast, to 30.4°N 123.9°W off Southern CCS), good agreement between the model and data is found for temperature, nitrate, and chlorophyll-*a* (Chl-*a*) concentrations. In particular, the cross-shore shape of the 13°C isotherm (Figures 3a and 3b), the 5 mmol N $m^{-3}$ isoline of nitrate (Figures 3c and 3d) and the subsurface maximum of Chl-*a* (Figures 3e and 3f) are accurately reproduced. In particular, the Chl-*a* maximum is dominated by large phytoplankton (diatom-like) close to the shore, and by small phytoplankton (non-diatom-like) offshore, as commonly observed in this region (e.g., line 80 [*Li et al*., 2010]). Some differences, such as a deeper Chl-*a* maximum (~10 m) in our model and the underestimation of the deep nitrate concentration and coastal Chl-*a* observed in Figures 3c–3f were also observed in the 15 km resolution model. They are related to the inability of the model to accurately represent the mean pathways and/or transformations of upwelling waters [*Chenillat et al*., 2013]. However, they do not call into question the ability of this model to reproduce realistic mesoscale dynamics

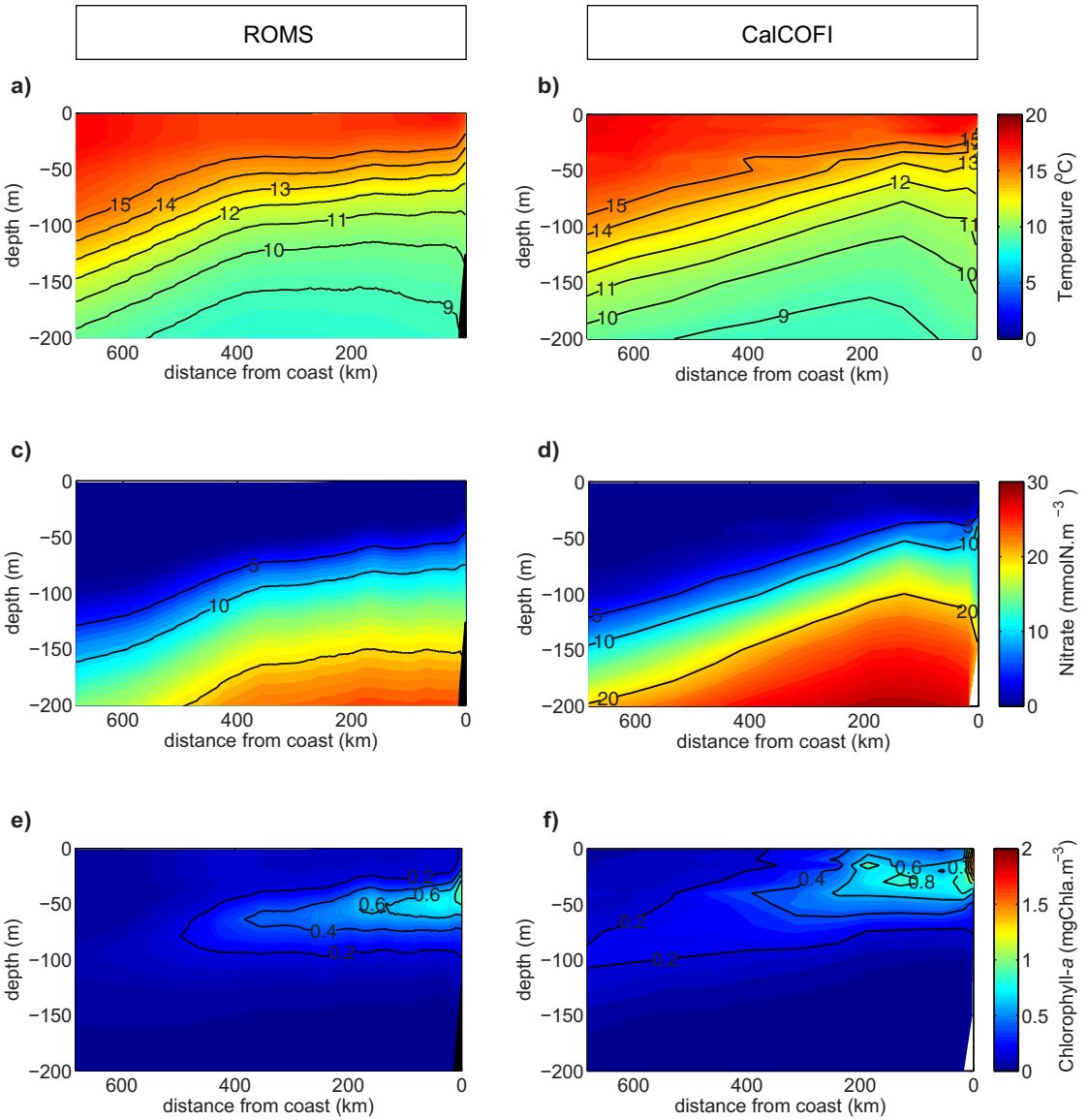


**Figure 3.** Comparison of the model with CalCOFI line 90. Annual mean vertical sections for the model (left) and observations (right) of (a and b) temperature (°C), (c and d) nitrate concentration (mmol N $m^{-3}$), and (e and f) Chlorophyll-*a* concentration (mg Chl-*a* $m^{-3}$).

[*Capet et al*., 2008; *Kurian et al*., 2011]. In particular, the latter study provides a favorable assessment of the realism of mesoscale eddy characteristics in the simulation.

In this study, we focus on one particular cyclonic eddy. Similar cyclonic eddies have been observed in this region and at the same time of the year [e.g., *Mantyla et al*., 2008], based on physical properties such as *SSH*, and biological properties such as Chl-*a* (Figure 4). The model phytoplankton biomass (total of *PS* and *PL*, in mmol N $m^{-3}$) has been converted to Chl-*a* using the same methodology as in *Chenillat et al*. [2013], based on the Chl-*a* to carbon conversion of *Cloern et al*. [1995]. Satellite images of Chl-*a* from SeaWiFS/MODIS (Sea-viewing Wide Field-of-view Sensor/Moderate Resolution Imaging Spectroradiometer on the NASA Aqua satellites) and our modeled surface Chl-*a* concentrations show similar patterns and contrasts, with high values of Chl-*a* inside the cyclonic eddy compared to the eddy exterior (Figure 4), with a similar range of values (0.25–0.75 mg Chl-*a* $m^{-3}$) [*Mantyla et al*., 2008]. Additionally, waters of the eddy and eddy exterior show low Chl-*a* concentrations typical of cyclonic eddies [e.g., *Haury et al*., 1978; *The Ring Group*, 1981; *Crawford*, 2005; *Crawford et al*., 2005; *Benitez-Nelson et al*., 2007; *Moore et al*., 2007; *Dietze et al*., 2009; *Peterson et al*., 2011; *Almazán-Becerril et al*., 2012], while the coastal region is characterized by higher values (>0.5 mg Chl-*a* $m^{-3}$) driven by upwelled nutrient-rich water [*Morales et al*., 2012].

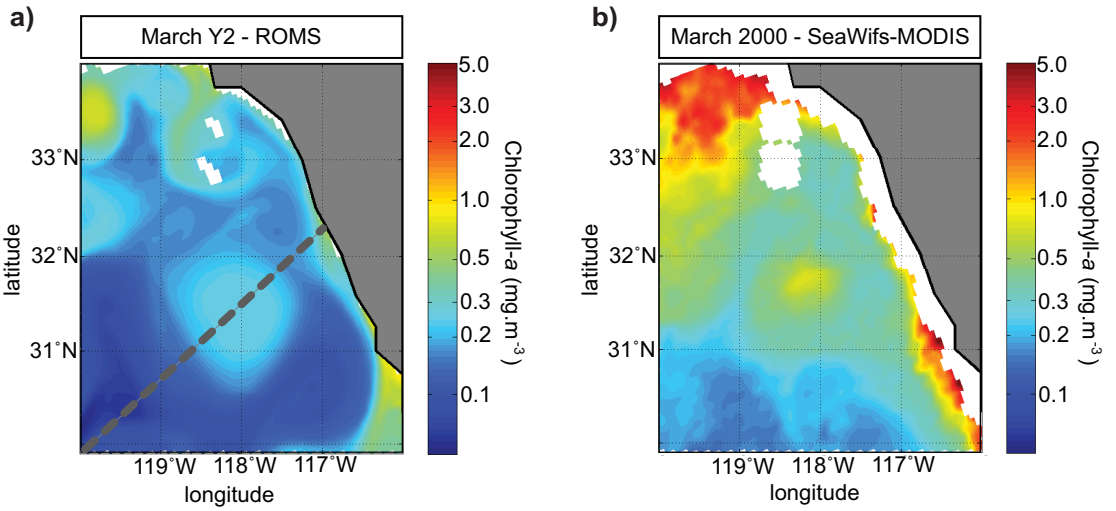


**Figure 4.** Monthly mean surface Chlorophyll-*a* concentrations (mg Chl-*a* $m^{-3}$) from (a) the model for March Y2 and (b) SeaWIFS for March 2000. The grey-dashed line in Figure 4a indicates the location of the cross-shore section of Figure 5.

Despite the differences between our model and observations, the coupled model is able to reproduce dynamics of the CCS including the eddy mesoscale activity and the mean biogeochemical patterns—in particular the Chl-*a* concentrations. In the next sections, we describe in detail the ecosystem structure inside the eddy, and compare it to waters of the eddy exterior and coastal region (Figure 2), analyzing the mechanisms involved in maintaining the high Chl-*a* concentrations in the eddy core.

## 4. Biological Patterns and Ecosystem Structure

### 4.1. Cross-Shore Patterns

Vertical sections across the eddy, from the coast at 32.3°N to 120°W-30°N, show the upward doming of the nitracline (Figure 5a), temperature, and salinity (not shown), typical of cyclonic eddies [*Yentsch and Phinney*, 1985; *Falkowski et al*., 1991]. Most significantly, both Chl-*a* concentrations (from total phytoplankton biomass, *PS*+*PL*) and total zooplankton biomass (*ZS*+*ZL*+*ZP*) have a subsurface maximum at the depth where the nitracline enters the euphotic zone in the eddy (Figures 5b and 5c). The associated shallower subsurface maximum of biomass is consistent with in situ observations of most cyclonic eddies [*The Ring Group*, 1981; *Falkowski et al*., 1991; *Benitez-Nelson et al*., 2007; *Nencioli et al*., 2008], including eddies in upwelling areas [*Nishimoto and Washburn*, 2002; *Moore et al*., 2007; *Peterson et al*., 2011; *Brzezinski and Washburn*, 2011; *Almazán-Becerril et al*., 2012; *Stramma et al*., 2013]. This enhanced subsurface maximum in the core of the eddy compared to the eddy exterior is likely driven by local upwelling of nutrients across the domed isopycnals, which sustains high local production [*Falkowski et al*., 1991; *Mcgillicuddy et al*., 1998; *Siegel et al*., 1999]. Indeed, within the eddy, the 100 m depth horizontal velocity amplitude is about 60% of the surface amplitude showing that the overall eddy depth reaches deep, nutrient-rich water, i.e., deeper than the euphotic zone.

The subsurface Chl-*a* maximum in the eddy core contrasts with those of the eddy exterior waters ~75 km and 250 km off the coast, where the isolines of nitrate are deeper and both Chl-*a* concentration and total zooplankton biomass are lower than in the eddy [*Haury et al*., 1978; *The Ring Group*, 1981; *Crawford*, 2005; *Crawford et al*., 2005; *Benitez-Nelson et al*., 2007; *Moore et al*., 2007; *Dietze et al*., 2009; *Peterson et al*., 2011: *Almazán-Becerril et al*., 2012]. In the 30 km band at the coast, the effects of coastal upwelling are apparent: the nitracline is shallow and enters the euphotic zone, inducing high primary production; Chl-*a* is higher, and zooplankton concentration is lower than in the eddy core [*Morales et al*., 2012].

By following the time-evolution of these biological distributions—separately for each class—we will compare and contrast the planktonic ecosystem structures of these different regions.

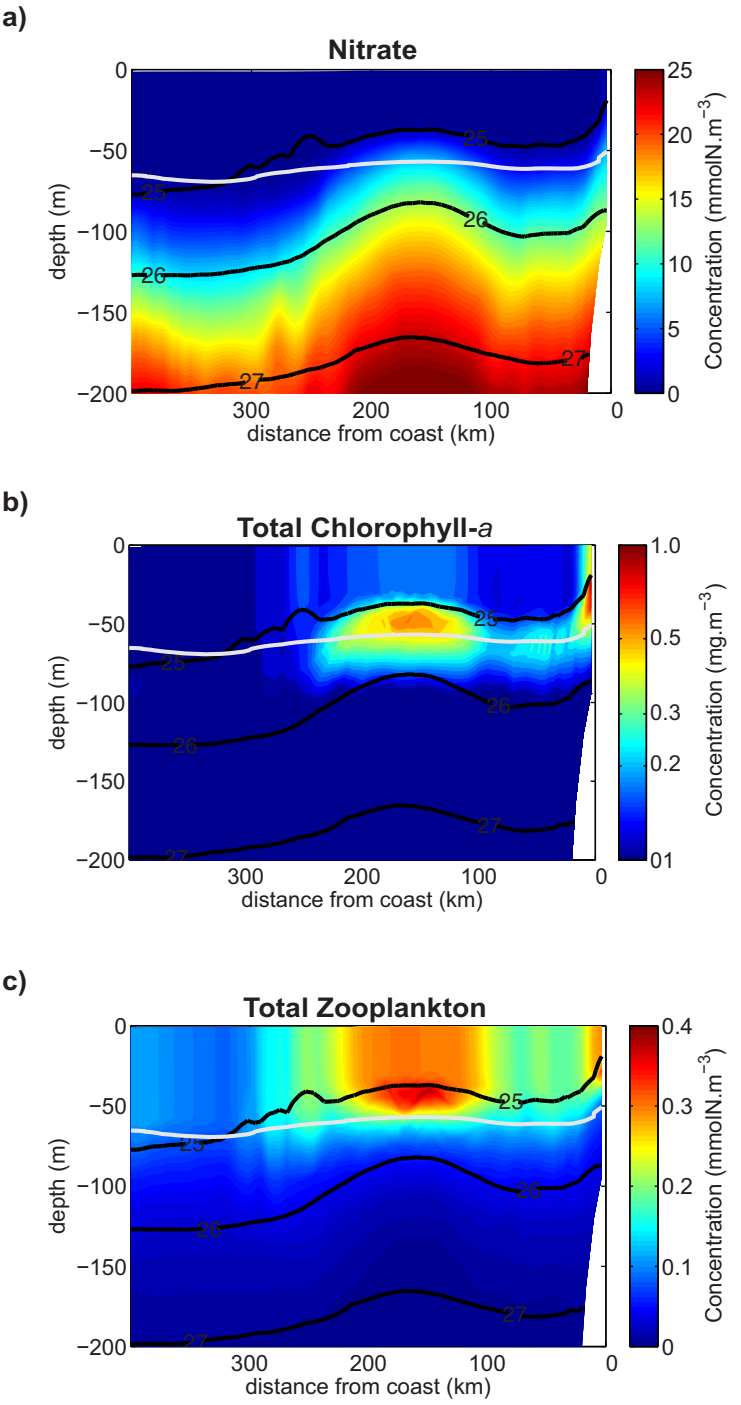


**Figure 5.** Cross-shore sections, across the cyclonic eddy on 30 March Y2 (location shown in Figure 4a). Model concentration of (a) nitrate (in mmol N m$^{-3}$), (b) total Chlorophyll-*a* (mg Chl-*a* m$^{-3}$), and (c) total zooplankton concentration (in mmol N m$^{-3}$). The isolines of density (in black) and the euphotic layer depth (in white) are superimposed.

### 4.2. Evolution of the Ecosystem: Region Comparison

To facilitate comparison of the concentrations of key biological variables, the properties were depth integrated over $z_{euph}$ and averaged over each region—the eddy core, the eddy exterior, and the coastal region (Figure 6).

When the eddy formed at the coast in November Y1, the ecosystem structure in the eddy core was similar to the ecosystem in the coastal upwelling region, with a comparable total nitrogen concentration of ~130 mmol m$^{-2}$. Nitrate dominated the total nitrogen (sum of organic and inorganic matter) concentrations with

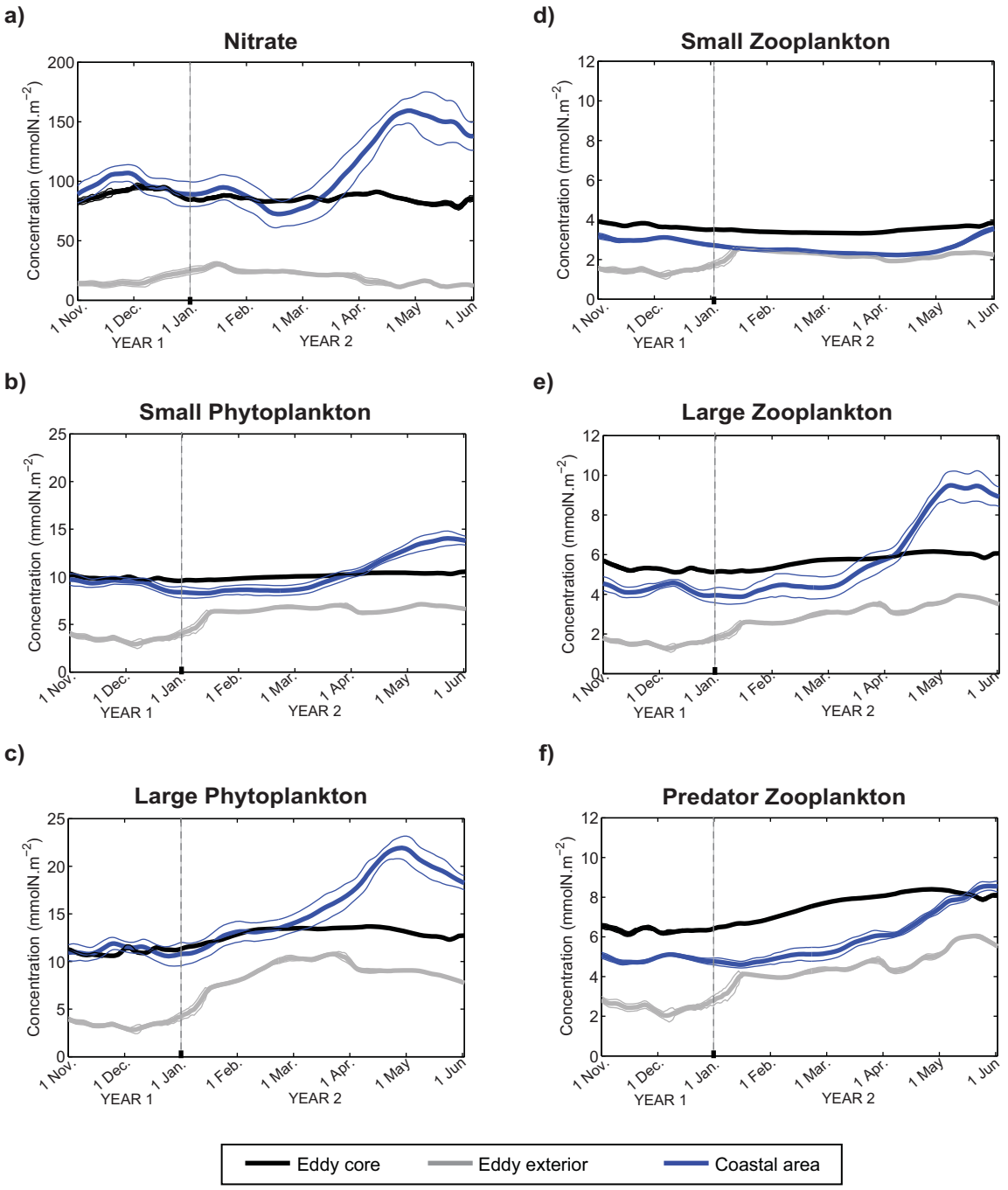


**Figure 6.** Time evolution of (a) nitrate, (b) small phytoplankton (PS), (c) large phytoplankton (PL), (d) small zooplankton (ZS), (e) large zooplankton (ZL), and (f) zooplankton predators (ZP). Units are in mmol N m$^{-2}$. These biological concentrations are integrated over the euphotic layer, and averaged horizontally over each domain of interest: the eddy core area (black bold solid lines), the eddy exterior area (grey bold solid lines), and the coastal area (blue bold-dashed lines). Standard deviations are represented as the daily spatial variability over the domain (thin solid lines): the low variability over the eddy core area reflects the spatial homogeneity of concentrations in this domain; the high variability of coastal upwelling concentrations is due to the spatial extent of the domain and the heterogeneity of concentrations.

80 mmol N m$^{-2}$ (Figure 6a), and despite the slight differences between the two regions in the concentrations of all the planktonic classes, their relative proportions were equal: the phytoplankton was 47% *PS* and 53% *PL* (Figures 6b and 6c), and the zooplankton 24% *ZS*, 35% *ZL*, and 41% *ZP* (Figures 6d, 6e, and 6f). These similarities in community structure were due to the trapping of large amounts of upwelled coastal waters in

the eddy core [*Flierl*, 1981; *Beckenbach and Washburn*, 2004; *Early et al*., 2011; *Almazán-Becerril et al*., 2012]; these waters account for 93% of the total core water.

While the eddy continued to grow and move offshore, the total nitrogen concentration remained relatively constant at ~131 mmol $m^{-2}$ in its core, whereas the relative proportions of biological components varied from their initial conditions. From 1 November Y1 to the middle of April Y2, total phytoplankton and zooplankton concentrations both increased by ~13% in the eddy, the percentage of large phytoplankton increased (42% *PS* and 58% *PL*), and the zooplankton community was partitioned into 19% *ZS*, 34% *ZL*, and 47% *ZP*. Though the integrated nitrate decreased about 10%, the small plankton classes *PS* and *ZS* tended to stay relatively constant, while the concentration of large organisms increased until the end of April Y2 by ~20% for *PL*, ~16% for *ZL*, and ~34% for *ZP*. This differential response among size classes reveals a shift in the ecosystem structure as the eddy matured toward a majority of large organisms, especially for *ZP*. Similar patterns have been observed previously in various cyclonic eddies formed at the coast: following these eddies over 2–3 weeks, Chl-*a* concentration remained relatively constant or slightly increased [*Bibby et al*., 2008; *Brown et al*., 2008], and large zooplankton species became dominant [*Goldthwait and Steinberg*, 2008; *Landry et al*., 2008b]. However, differences in the phytoplankton community size structure among eddies appears to be due to the local nutrient availability and/or the stage of eddy development [*Sweeney et al*., 2003]. Both these factors are correlated with physical and biological dynamics, e.g., nutrient fluxes linked to eddy dynamics [*Brown et al*., 2008; *Nencioli et al*., 2008], and rate of photosynthesis or grazing pressure by zooplankton [*Landry et al*., 2008a]. In our model, such information is available and continuous over longer periods, allowing us to understand and quantify the mechanisms responsible for such structural changes in the ecosystem.

Both the composition and the concentrations of the planktonic classes in the eddy departed from those of the coastal upwelling region after March Y2. At the coast, all the concentrations increased significantly and the total nitrogen concentration reached ~230 mmol $m^{-2}$—much more than in the eddy core (as in *Morales et al*. [2012])—in conjunction with enhanced coastal upwelling in late winter/early spring. The resulting coastal ecosystem structure contained larger concentrations of *PL* and *ZL*, contrasting with the eddy core which had higher *ZP* concentrations.

Over the life of the eddy, biological concentrations in the eddy core were always much higher (by a factor of ~2–3) than in the oligotrophic eddy exterior waters. This observation is consistent with studies of other coastal eddies where this factor may vary up to 4 [*Benitez-Nelson et al*., 2007; *Bibby et al*., 2008; *Almazán-Becerril et al*., 2012; *Stramma et al*., 2013]. Total nitrogen concentrations in the eddy exterior waters were ~42 mmol $m^{-2}$—always lower than inside the eddy—showing a clear local effect of the presence of the eddy. There was low lateral mixing between waters of the eddy's core and its edge (Figures 1a and 1b), demonstrating the capacity of the eddy to maintain high biological concentrations at its core for several months.

This comparison of vertically integrated properties among regions is useful for elucidating differences in the ecosystem structure of the eddy's core compared to relevant noneddy regions. However, given the intense deep Chl-*a* and zooplankton maxima in the eddy (Figure 5), we might expect some vertical heterogeneity in the ecosystem response inside the eddy relative to the eddy exterior waters. Vertical gradients are often associated with planktonic assemblages dominated by large size classes in subsurface water (driven by local nutrient inputs), contrasting with a dominance of small size classes in the surface mixed layer [*Brown et al*., 2008].

### 4.3. Evolution of the Vertical Structure in the Eddy Core

Vertical profiles of biological variables and total nitrogen in the ecosystem averaged over the eddy core (Figure 7) demonstrate the decoupling of the mixed layer (ML) from the subsurface layer (between the bottom of the ML and the euphotic depth), with low (high) concentrations at the surface (subsurface) [*Bibby et al*., 2008; *Landry et al*., 2008b]. The depths of these two layers changed over time through seasonal changes of the ML. The initial 14 m depth of the ML in the eddy core in November Y1 deepened to 41 m in February Y2, then shoaled to 20 m in June Y2, consistent with higher mixing in winter followed by spring stratification. The euphotic depth did not change a great deal over time and remained at ~60 m (Figure 7), i.e., 20 m or more deeper than the base of the ML. This does not allow nutrient replenishment of the ML by vertical mixing, even during winter.

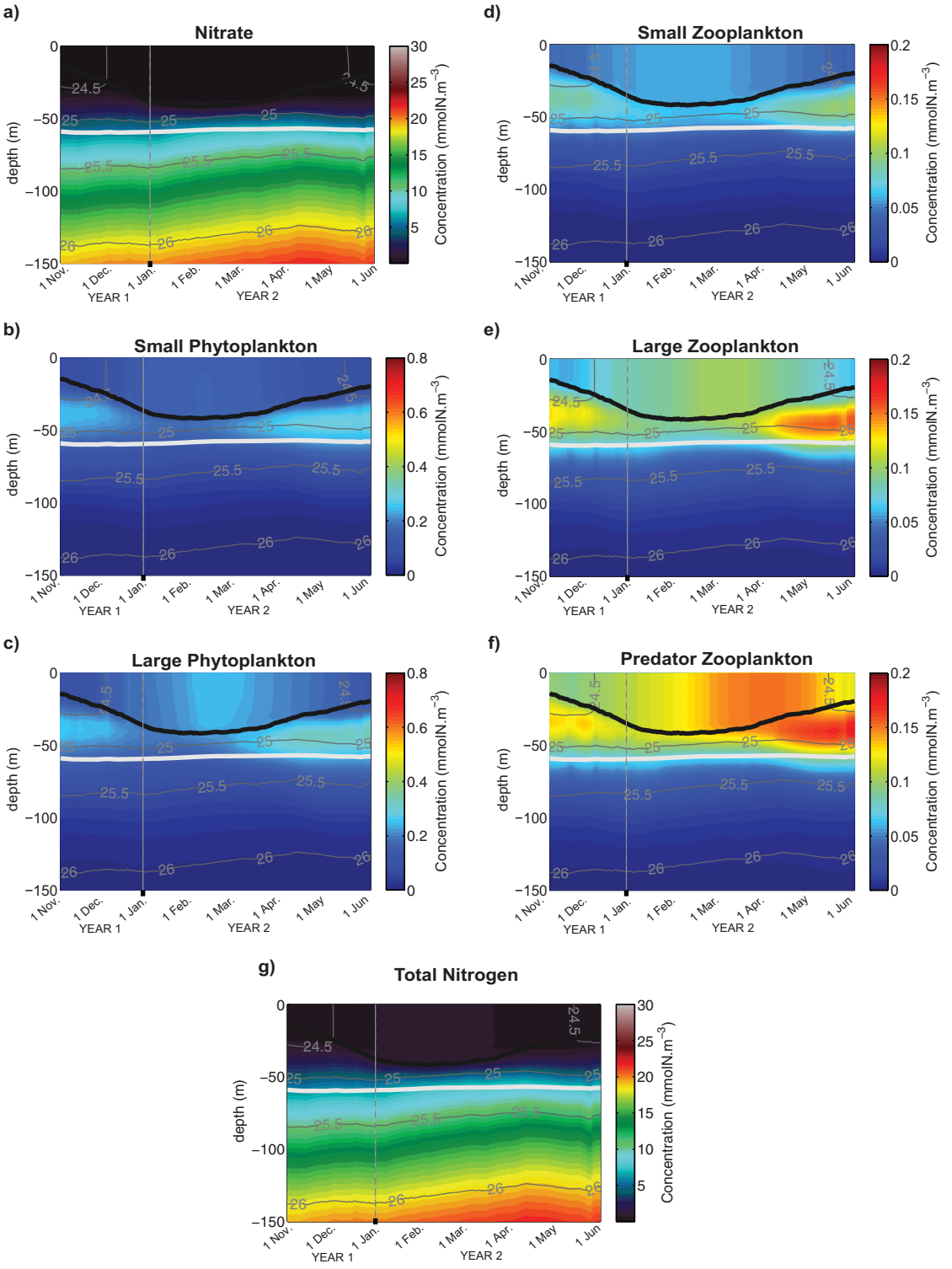


**Figure 7.** Time evolution of the main biological vertical concentration profiles averaged in the eddy core: (a) nitrate, (b) small phytoplankton (PS), (c) large phytoplankton (PL), (d) small zooplankton (ZS), (e) large zooplankton (ZL) (f) zooplankton predators (ZP), and (g) total nitrogen summed over the ecosystem. Units are mmol N m$^{-3}$. The density (grey lines), the mixed layer (ML) depth (black bold line), and the euphotic layer depth (white bold line) are superimposed.

Though the ML in the eddy core showed low nitrate concentrations compared to subsurface waters (Figure 7a), there was a clear planktonic response to changes in the ML depth (Figures 7b–7f). As the eddy formed at the coast in November Y1 and the ML deepened, the initially low surface planktonic concentrations

increased by factors of 5.6 and 4 for the phytoplankton and the zooplankton, respectively (Figures 7b–7f). Most of this increase was in the larger size classes, which showed sequential peak abundances: *PL*, *ZL*, and *ZP* concentrations peaked in January, February, and March Y2, respectively. The *PS* and *ZS* concentrations remained relatively constant during eddy formation. As the eddy propagated offshore, there was a decrease of all planktonic concentrations at the surface. This decrease could be related to either the normal seasonal cycle of the offshore ecosystem or to the time since the eddy core and associated ecosystem became isolated from their eddy exterior water masses (Figures 1a and 1b). Such a decrease of surface concentrations of Chl-*a* with the age of the eddy has been seen in cyclonic eddies of the CCS using satellite data (M. D. Ohman, K. Barbeau, R. Goericke, M. R. Landry, and A. J. Miller, *Ecological Transitions in the California Current Ecosystem: CCE-LTER Phase II*, unpublished material, 2010) [*Gaube*, 2012]. However, the satellite data miss critical details of the subsurface dynamics of the primary producers [*Chelton et al*., 2011b].

In exploring the subsurface patterns, we focus on the ecosystem response between the bottom of the ML and the base of the euphotic zone in the eddy's core. Nitrate concentrations here were 10 times higher than at the surface, and the nitracline depth shoaled into the euphotic zone as the eddy moved offshore, until March Y2 (Figure 7a). This shoaling nitracline led to large increases in the subsurface plankton concentrations from March to April Y2 for phytoplankton and April to May Y2 for zooplankton (Figures 7b–7f). The response of the ecosystem is clear in examining the total nitrogen of the system (Figure 7g): the main signal is an upward lifting of the deep nitrogen pool that followed the shoaling nitracline (Figure 7a). The delay between peaks in the different size classes is shorter in the subsurface layer than in ML, reflecting vertical differences in the response of the ecosystem to local forcing in the eddy core.

In situ data of cyclonic mesoscale features in EBUS are relatively sparse, but recent sampling in various systems has provided evidence of subsurface maxima of phytoplanktonic assemblages [e.g., *Bibby et al*., 2008; *Almazán-Becerril et al*., 2012]. The observed assemblages varied with the distance of the eddy from the coast, which is correlated with the eddy age [*Rii et al*., 2008]. The different phytoplanktonic assemblages were found to vary with changes in the degree of remineralization inside the eddy and the local nutrient supply [*Brown et al*., 2008; *Rii et al*., 2008] or the differential planktonic response to the environment [*Almazán-Becerril and Garcìa-Mendoza*, 2008; *Suggett et al*., 2009; *Almazán-Becerril et al*., 2012]. Moreover, these subsurface maxima of phytoplanktonic assemblages in cyclonic eddies were associated with high photosynthetic rates [e.g., *Bibby et al*., 2008; *Almazán-Becerril et al*., 2012]. These rates were stimulated by high nutrient concentrations associated with the shoaling of the nitracline into the euphotic layer.

To identify and quantify the mechanisms driving the biological response inside the cyclonic eddy, we now focus on the biological and physical fluxes controlling the sources and sinks of biological material, including recycling of organic matter inside the eddy.

## 5. Physical-Biological Dynamics

### 5.1. Biological Fluxes and Ecosystem Functioning

Our goal is to understand the mechanisms driving the ecosystem changes in the eddy core. We saw that when the eddy core formed and detached from the coast, it evolved independently of its source waters and the eddy exterior waters (see section 4). Over the months of offshore transport, sinking organic matter would be expected to induce a decrease in biological concentrations in the eddy [*Gruber et al*., 2011]. Instead, we observed sustained high biomass, and even an increase in the large size classes. In this section, we analyze the biological fluxes driving exchanges of nutrients among the biological compartments.

In the eddy core, the time-averaged total primary production of 1.60 mmol N $m^{-2}$ $d^{-1}$ was comprised of 40% ammonium ($NH_4^+$) uptake (0.65 mmol N $m^{-2}$ $d^{-1}$), and 60% nitrate ($NO_3^-$) uptake (0.95 mmol N $m^{-2}$ $d^{-1}$) (Figures 8a and 8b). While the eddy moved offshore, total primary production first decreased slightly then increased, though the ratio of $NO_3^-$ to $NH_4^+$ uptake remained constant. Nutrients are made available through recycling, fueling regenerated production, or they can be brought into the euphotic layer through physical processes, fueling new production [*Dugdale and Goering*, 1967]. To understand nutrient uptake dynamics, we begin by quantifying the biological sources of $NO_3^-$ and $NH_4^+$.

$NH_4^+$ concentrations in the ocean are low except in biologically productive areas where there can be a large contribution from the remineralization of detritus. In our ecosystem model, $NH_4^+$ is produced by egestion

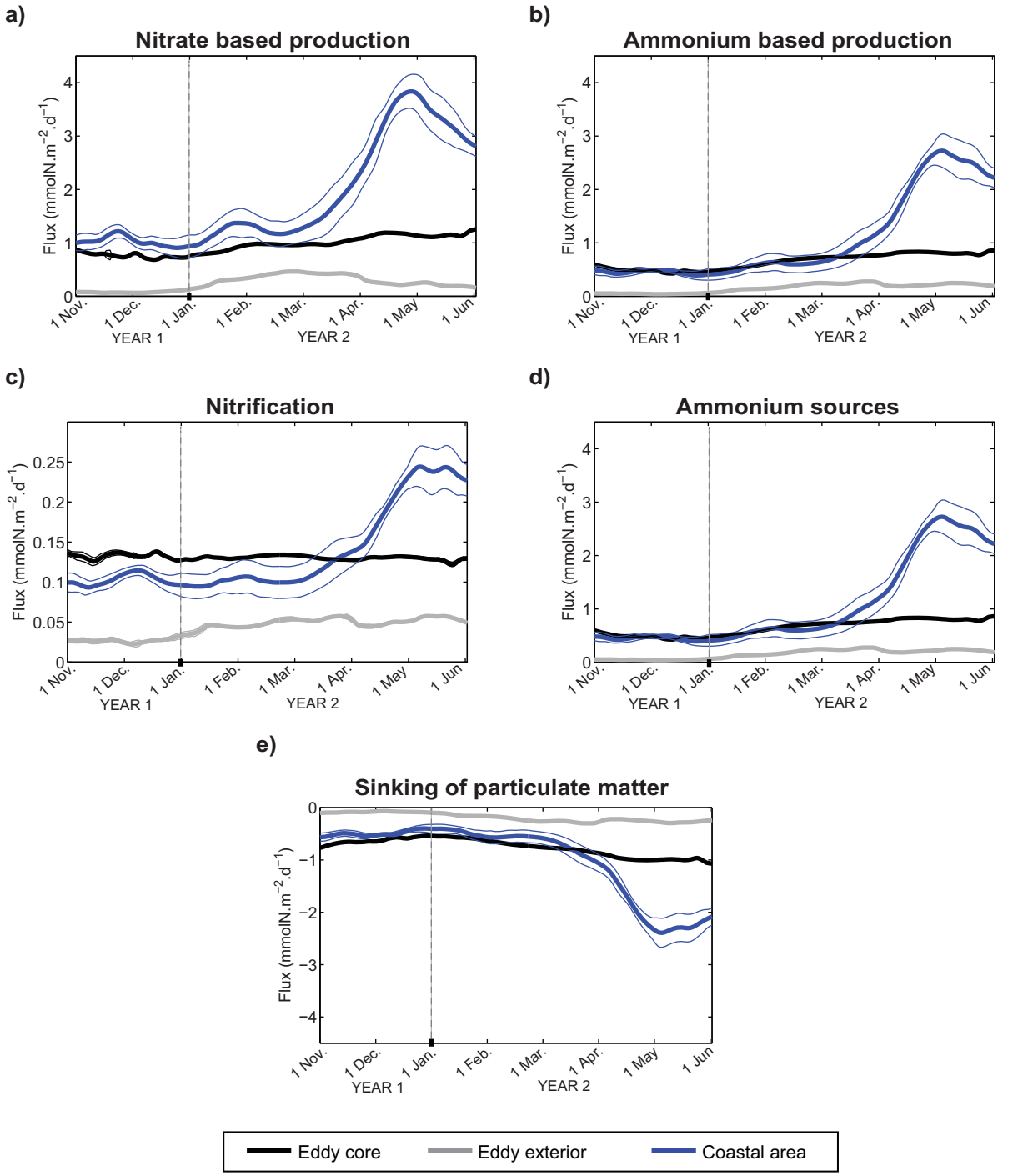


**Figure 8.** Time evolution of some biological fluxes, integrated over the euphotic layer, and averaged over the eddy core (black bold solid lines), the eddy exterior area (grey bold solid lines), and the coastal area (blue bold dashed lines): (a) production based on nitrate, (b) production based on ammonium, (c) nitrification, (d) total ammonium sources (from egestion by zooplankton, and recycling of dissolved and particulate matters), and (c) sinking of particulate matter. Units are mmol N m$^{-2}$ d$^{-1}$. Standard deviations are given as the daily spatial variability over the domain (thin solid lines).

by the zooplankton and recycling of dissolved and particulate forms of nitrogen (Figure 8d). In the eddy core, all these sources increased over time, with contributions of 70% egestion (an average of 0.54 mmol N m$^{-2}$ d$^{-1}$), 16% recycling of dissolved nitrogen (0.12 mmol N m$^{-2}$ d$^{-1}$), and 14% recycling of particulate nitrogen (0.11 mmol N m$^{-2}$ d$^{-1}$).

Because of photosynthetic uptake in the euphotic zone and remineralization of sinking organic material in deep water, $NO_3^-$ concentrations tend to be low in the euphotic zone and high in deep water (Figure 7). The only biological source of $NO_3^-$ in the model is nitrification of $NH_4^+$; uptake of this "recycled" $NO_3^-$ must be counted as part of the recycled production (the other part being fueled by $NH_4^+$). In the eddy core, nitrification (Figure 8c) was low (0.13 mmol N $m^{-2}$ $d^{-1}$ on average) compared to the total biological uptake of nitrogen (1.60 mmol N $m^{-2}$ $d^{-1}$) (Figures 8a and 8b). Thus biological sources of $NO_3^-$ through nitrification cannot account for the observed total $NO_3^-$ biological uptake (0.95 mmol N $m^{-2}$ $d^{-1}$) at the eddy core.

In contrast, the sinking of particulate matter (0.76 mmol N $m^{-2}$ $d^{-1}$ on average) (Figure 8e), which drives a loss of nitrogen from the eddy core, is about half the total primary production of 1.60 mmol N $m^{-2}$ $d^{-1}$ (Figures 8a and 8b). Thus, the combination of sinking and biological fluxes cannot lead to a balanced biological system: nitrogen concentrations would decrease in the eddy core. Clearly, to maintain the elevated total nitrogen concentrations in the eddy core there must be a source of nitrate driven by physical processes.

### 5.2. Vertical Advection of Nitrate

Mesoscale features are known for their locally enhanced vertical velocities at their formation [*Sweeney et al*., 2003]. In particular, in cyclonic eddies we expect to observe shoaling isopycnals and an upward advective flux of nitrate driven by upward vertical velocities acting on enhanced deep nitrate concentrations [*Mcgillicuddy et al*., 1998, 2007; *Nishimoto and Washburn*, 2002; *Benitez-Nelson et al*., 2007; *Moore et al*., 2007; *Brzezinski and Washburn*, 2011; *Peterson et al*., 2011]. However, according to *Sweeney et al*. [2003] when an eddy reaches its "mature" phase, it evolves in solid body rotation and vertical advective inputs are limited. This hypothesis was revisited by *Nencioli et al*. [2008] using in situ observations: they suggest that during this "mature" phase, local nutrient upwelling occurs while the eddy translates horizontally. Our results suggest that the advective shoaling of the nitracline into the euphotic zone (Figure 7a) could explain the difference between the total nitrate uptake and production based on nitrate made available through nitrification in the eddy's core (Figures 8a and 8c).

Analyses of the model show that the average vertical flux of nitrate in the core of the eddy was 0.79 mmol N $m^{-2}$ $d^{-1}$, with negligible horizontal ($-0.04$ mmol N $m^{-2}$ $d^{-1}$) and diffusive (0.05 mmol N $m^{-2}$ $d^{-1}$) fluxes. The nitrate input to the euphotic zone is considerably lower in eddy exterior waters (0.17 mmol N $m^{-2}$ $d^{-1}$), though much higher in the coastal region (2.04 mmol N $m^{-2}$ $d^{-1}$) due to coastal wind-driven upwelling (Figures 6a and 9).

Much of the vertical advection of nitrate is driven by Ekman pumping acting on the shallow nutricline in the eddy [*Martin and Richards*, 2001; *McGillicuddy et al*., 2007]. The pumping itself ($W_E$) represents a local upwelling driven by the surface wind stress curl $\nabla\times\tau$. In the core of the eddy, $W_E$ was estimated to be $\sim 0.13 \pm 0.04$ m $d^{-1}$, (computed from 1 January to 1 June Y2, when the net vertical advective flux was positive); this is the same order of magnitude as in the eddy exterior waters ($\sim 0.09 \pm 0.07$ m $d^{-1}$). This velocity corresponds to $\sim$20 m in 6 months (the eddy lifetime) which is modest. However, the vertical nitrate flux is driven by the product of $W_E$ and the local nitrate concentration. In the eddy core, the nitrate flux is enhanced due to the high nitrate concentrations at shallow depths driven by the domed isopycnals (and isolines of nitrate) shaping the cyclonic eddy. Outside the eddy, the low vertical advective flux of nitrate to the euphotic zone mainly reflects the deep nitracline—deeper than $z_{euph}$. Even though vertical velocities at the base of the euphotic layer are, on average, slightly higher outside the eddy than within the eddy core (0.15 m $d^{-1}$ versus 0.10 m $d^{-1}$ in the eddy core), the nitrate concentrations there are so low (20.0 mmol N $m^{-2}$ versus 86.6 mmol N $m^{-2}$ in the eddy core) that the net vertical advective nitrate flux is low. Note that within the eddy core, the variability of the vertical velocity is half that outside the eddy where a mixture of processes occurs. The Ekman pumping simply lifts nutrients up; it is the shoaling of the nitracline into the euphotic layer due to the presence of the cyclonic eddy that allows the enhanced nitrate flux into the euphotic zone of the eddy core. The presence of the eddy (the doming of the isopycnals and nitrate isopleths) predisposes the Ekman pumping to be capable of advecting nitrate into the euphotic zone.

Eddy-wind interactions also can dampen eddy-induced upwelling in cyclonic eddies through an air/sea interaction driven by the feedback of the eddy rotation to the wind stress curl, reducing the effective wind stress curl [*Martin and Richards*, 2001; *McGillicuddy et al*., 2007]. By reducing $W_E$, these eddy-wind interactions would decrease the local input of nitrate and the strength of the biological response in cyclonic eddies. This mechanism is not taken into account in our model, but in the CCS this eddy/wind interaction

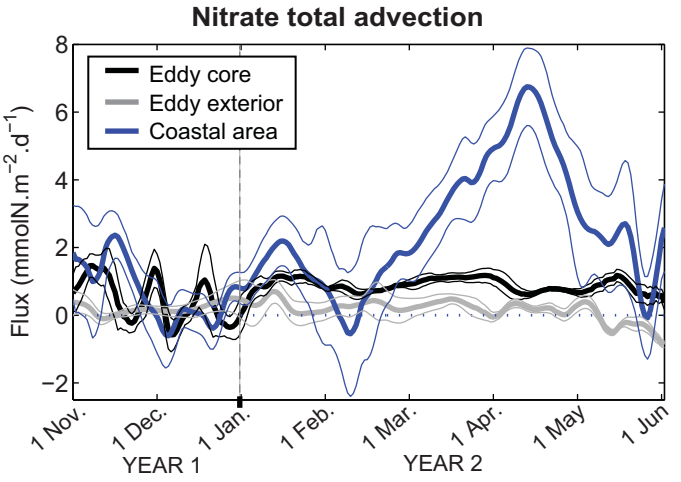


**Figure 9.** Time evolution of the vertical advective nitrate flux integrated over each domain of interest: the eddy core (black lines), the eddy exterior area (grey lines), and the coastal area (blue lines). A 5 day moving average has been applied to smooth the signal. Units are mmol N $m^{-2}$ $d^{-1}$.

was shown to be small, with a downwelling of O(0.01) m $d^{-1}$, [*Gaube*, 2012] compared to the upwelling velocities of O(0.10) m $d^{-1}$ observed in our cyclonic eddy.

In this model, we also neglect the potential nutrient fluxes driven by nonlinear Ekman pumping. Nonlinear Ekman pumping mainly occurs at the submesoscale, in response to sharp vorticity gradients [*Stern*, 1965; *Thomas and Rhines*, 2002; *Mahadevan et al*., 2008], but mainly around the eddy edges [*Klein and Lapeyre*, 2009], where vertically displaced water is redistributed to the eddy core by advection [*Mahadevan et al*., 2008]. We verified that nonlinear processes are negligible in our model (ratio of the relative vorticity to the Coriolis term is $\ll 1$) suggesting that our estimate of Ekman pumping is well represented by the linear component.

Given that vertical advection is the main source of locally enhanced nitrate fluxes into the euphotic zone, it is important to explore how this enhanced flux influences the vertical structure of local production.

### 5.3. Vertical Decoupling of Biological Production

As mentioned earlier, planktonic groups in the eddy core show segregation between the ML and the subsurface layer, with their concentrations evolving differently through time (Figure 7). Here we analyze new and regenerated primary production, ecosystem function, and differential ecosystem responses in the ML and in the subsurface layer. In this section, ratios, fluxes and specific rates are given as temporal averages over the period of analysis, and depth-averages over the layer mentioned (euphotic layer, mixed layer, or subsurface layer).

We can assume that nutrients—mainly $NO_3^-$—upwelled into the euphotic zone are directly utilized for new production (as in *Siegel et al*. [1999]). This assumption allows us to calculate an *f*-ratio [*Eppley and Peterson*, 1979], which represents the ratio of primary production driven by nutrient input into the euphotic zone ("new production") relative to the total primary production. We found an *f*-ratio of 0.5 in the eddy core over the entire euphotic zone, contrasting with *f*-ratios of 0.4 and 0.7 in the eddy exterior and coastal regions, respectively. The high coastal *f*-ratio is consistent with in situ data [*Chavez and Smith*, 1995] and reflects the significant nutrient supply by coastal upwelling, which sustains intense biological production there. Conversely, the *f*-ratio is lower in the eddy exterior waters, where the productivity is low. However, in the core of the eddy, the *f*-ratio is lower than might be expected according to preceding studies [*Allen et al*., 1996]; this is because it is averaged over the entire euphotic zone, reflecting the biological uncoupling between the ML and the subsurface layer (Figure 7).

In the ML, the total primary production reached its maximum in February Y2, with a depth-integrated (over the ML) time average of 0.63 mmol N $m^{-2}$ $d^{-1}$ (Figure 10c). This primary production was based mainly on $NH_4^+$ uptake (~60%), except from December Y1 to March Y2, when $NO_3^-$ uptake temporarily increased (up to 60%) (Figure 10b and 10c). In these oligotrophic conditions, nitrate originates equally from nitrification and vertical advection, (each 0.036 mmol N $m^{-2}$ $d^{-1}$), and to a lesser extent from diffusion (0.007 mmol N $m^{-2}$ $d^{-1}$). Vertical advection and diffusion of $NH_4^+$ were negligible (O($10^{-4}$) mmol N $m^{-2}$ $d^{-1}$). Thus, only 6% of the biological nitrogen uptake was supported by physical processes (advection and diffusion), and the *f*-ratio in the ML was <0.1. In the ecosystem model, all the nitrogen-specific recycling rates were constant, with a decomposition rate of particulate matter to $NH_4^+$ and dissolved matter of 0.2 $d^{-1}$, a recycling from dissolved matter to $NH_4^+$ of 0.04 $d^{-1}$ and a nitrification rate of 0.06 $d^{-1}$ [*Kishi et al*., 2007]. These

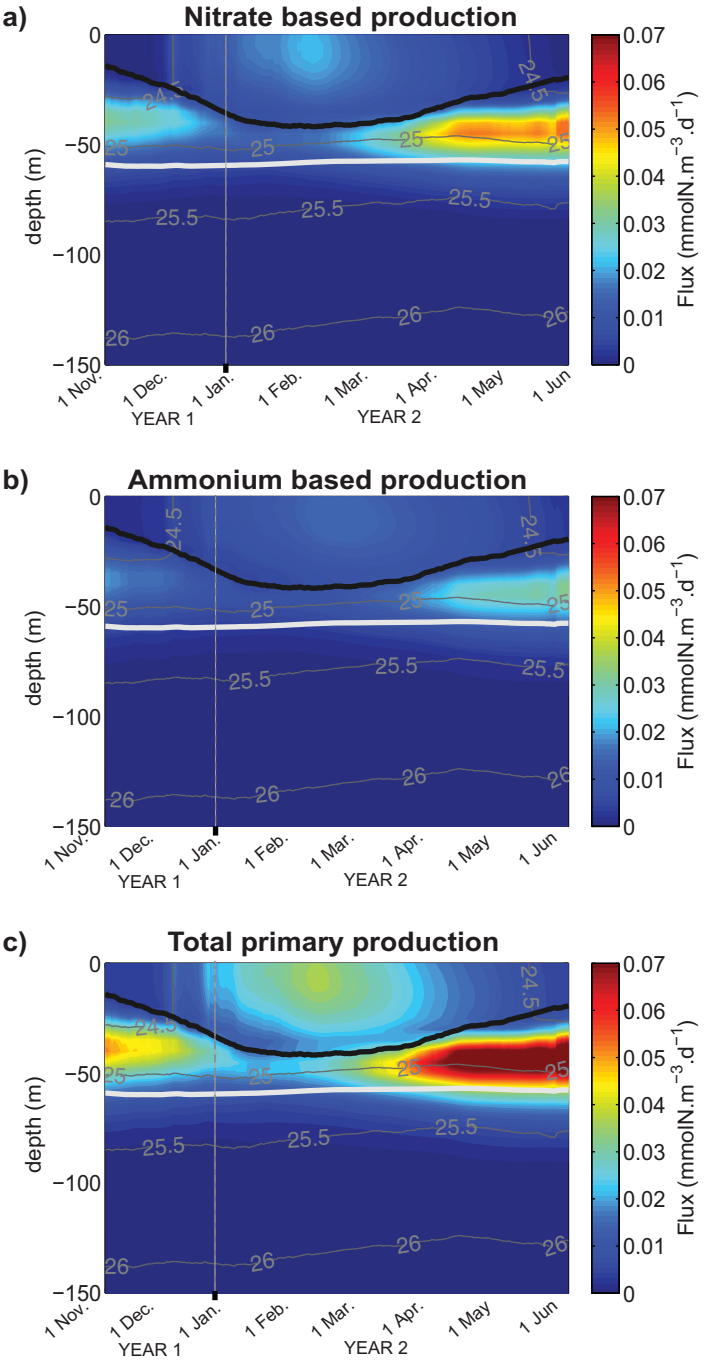


**Figure 10.** Time evolution of the vertical dependence of primary production averaged over the eddy core: (a) the production based on nitrate, (b) the production based on ammonium, and (c) the total primary production. The density (grey lines), the mixed layer (ML) depth (black bold line), and the euphotic layer depth (white bold line) are superimposed.

recycling rates are comparable to or greater than the nitrogen-specific phytoplankton growth rates (0.03 $d^{-1}$ and 0.06 $d^{-1}$ for *PS* and *PL*) or zooplankton grazing rates (0.04 $d^{-1}$, 0.08 $d^{-1}$, and 0.05 $d^{-1}$, respectively, for *ZS*, *ZL*, and *ZP*). This also suggests that in the ML the ecosystem is highly dependent on the regeneration of the coastal material initially present in the eddy. These concentrations ultimately limit the ML ecosystem functions, leading to a decline of concentrations through export of particulate matter by sinking.

In the subsurface layer, between the bottom of the ML and the base of the euphotic zone, the ecosystem is more productive than in the ML. During the life of the eddy, the depth-integrated time-averaged total

primary production was 1.0 mmol N $m^{-2}$ $d^{-1}$, with ~63% from $NO_3^-$ uptake and ~37% from $NH_4^+$ uptake (Figure 10). Much of the $NO_3^-$ was supplied by the vertical advective flux of 0.79 mmol N $m^{-2}$ $d^{-1}$, supporting an *f*-ratio of ~0.8, comparable with in situ data from cyclonic eddy cores [e.g., *Allen et al*., 1996]. This high primary production, dominated by new production due to the continuous vertical input of nitrate (Figure 11b), efficiently fueled the higher trophic levels [*Landry et al*., 2008b]. Indeed, though all the recycling rates are the same as in the ML, subsurface phytoplankton growth rates (0.07 $d^{-1}$ and 0.09 $d^{-1}$ for *PS* and *PL*) and zooplankton grazing rates (0.09 $d^{-1}$, 0.14 $d^{-1}$, and 0.07 $d^{-1}$ for *ZS*, *ZL*, and *ZP*, respectively) were much higher. In this subsurface layer, recycling is limited; high primary and secondary production is maintained by physical advection of nutrients (Figure 11a). Note that the total advection of nitrate (sum of horizontal and vertical advection) is mainly due to a vertical advection from below the euphotic layer (Figure 11b), while a weak lateral advective loss of nitrate occurs subsurface (Figure 11c). These vertically advected new nutrients appear to be trapped in this subsurface layer, leaving the surface ML decoupled from the subsurface layer, and dependent on recycled nutrients.

The fluxes of dissolved inorganic nitrogen demonstrate that the ecosystem functions quite differently in the surface and subsurface layers: biological activity is stratified in the water column [*Landry et al*., 2008b]. In the subsurface layer, the ecosystem dynamics were largely driven by the input of new nutrients as a result of continuous vertical advection of nitrate into the base of the euphotic zone (Figure 11b). This led to higher turnover rates in the subsurface layer compared to the surface layer: an increase of 150% for the larger size classes, and 230% for the smaller size classes. In the surface layer, the ecosystem is mainly based on recycled nutrients (originating from coastal material) with low nutrient input [see also *Almazán-Becerril et al*., 2012]. The vertical advective flux of nitrate induced a vertical bifurcation in ecosystem functioning in the core of the eddy: larger organisms dominating the subsurface layer were controlled by physical fluxes of new nutrients, while both small and large organisms at the surface relied on recycled nutrients originating from the eddy's coastal source, consistent with in situ observations of cyclonic eddies [*Brown et al*., 2008].

## 6. Horizontal Cross-Shore Transport Versus Vertical Local Input

Mesoscale dynamics drive both horizontal cross-shore transport and local vertical inputs [*Crawford*, 2005; *Feng et al*., 2007; *Moore et al*., 2007; *Brzezinski and Washburn*, 2011; *Lehahn et al*., 2011; *Peterson et al*., 2011; *Morales et al*., 2012]. Our analyses show that horizontal and vertical dynamics work together to control ecosystem functioning in the eddy core. Vertical advective inputs of nitrate to the eddy core drove locally enhanced new production that represented ~50% of the total primary production in the subsurface waters. Furthermore, the core of the eddy was formed with enhanced nutrient concentrations due to its coastal origin; these nutrients (~2/3 of the total nitrogen stock) plus those imported vertically by advection (~1/3 of the total nitrogen stock) were locally recycled through the ecosystem as the eddy moved offshore, with a portion lost through sinking. Of the nitrogen transported from the coast, we estimate that after 7 months ~1/2 was recycled through biological activities and ~1/2 sank with particulate material. We show that the sinking losses are locally compensated by a vertical input within the eddy driven by the Ekman pumping that lifts the domed nitracline up into the euphotic layer.

We found that for EBUS horizontal advection by eddies plays an important role in trapping coastal biological material, particularly at the surface within the core. Over several months this material was efficiently transported offshore with limited lateral exchange, and the biological activity was maintained despite some losses by vertical sinking. While the eddy travels offshore, vertical advection drives an enhanced flux of nitrate to subsurface waters at the core of the eddy. This subsurface enrichment does not affect the surface layer where trapped material is recycled. The subsurface enrichment locally enhances biological production as in in situ observations [e.g., *Morales et al*., 2011; *Stramma et al*., 2013]. The fact that subsurface particles located on the edge of the eddy remain trapped there for long periods of time strongly suggests that the leaky model proposed by *Nencioli et al*. [2008] does not apply here. In their model, advective and diffusive exchanges along isopycnals spread some of the primary production away from the eddy. In our case, the eddy structure remained coherent below the euphotic layer and isopycnal leakage is presumably weak (Figures 1a and 1b).

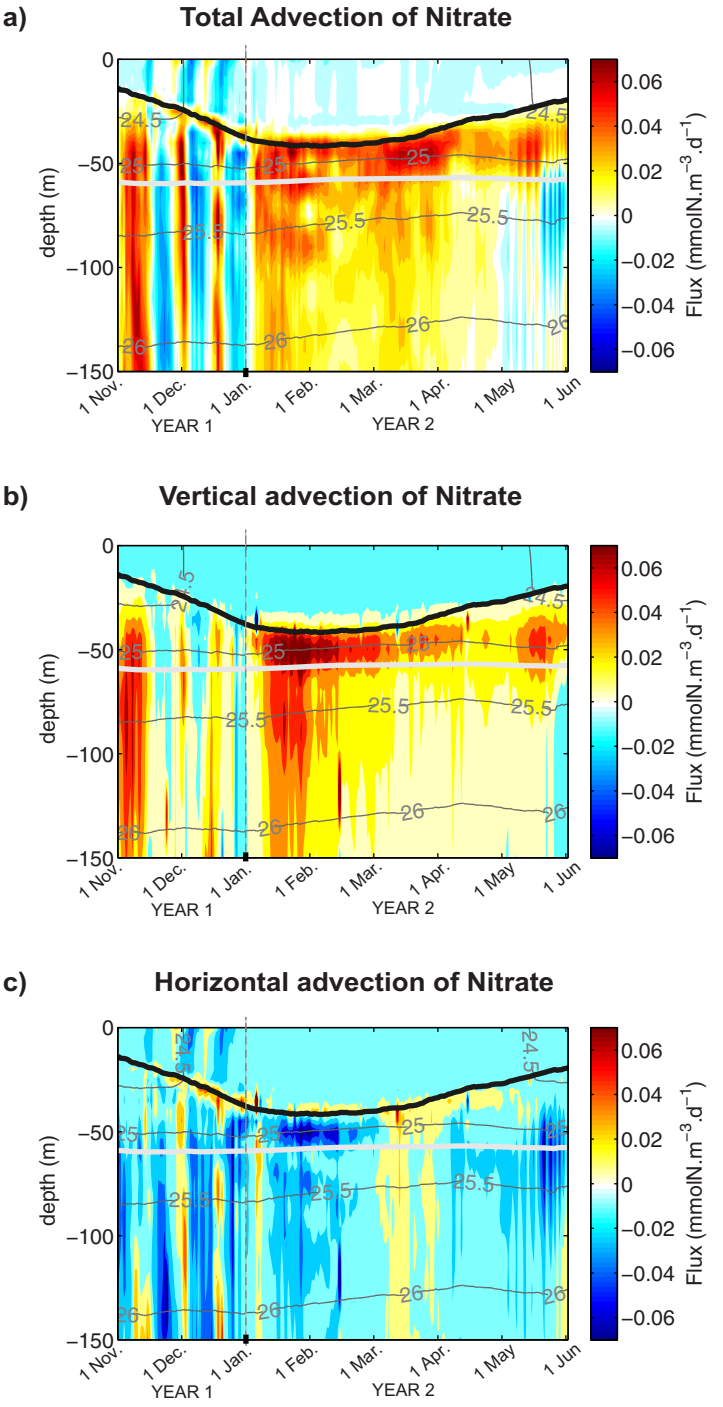


**Figure 11.** Time evolution of the vertical dependence of nitrate advection averaged over the eddy core: (a) the total advection, (b) the vertical advection, and (c) the horizontal advection. The density (grey lines), the mixed layer (ML) depth (black bold line), and the euphotic layer depth (white bold line) are superimposed.

Our results are based on a relatively simple ecosystem model, which facilitates the analysis of the complex mechanisms involved in the physical-biological interactions within an eddy. NEMURO is based on two phytoplankton size classes and three zooplankton size-classes [*Kishi et al*., 2007]; implementation of more complex planktonic size-class interactions would lead to better understanding of shifts in the planktonic community structure, from dominance by coastal species to open ocean species [*Brown et al*., 2008;

*Almazán-Becerril et al*., 2012; *Stramma et al*., 2013]. However, running such a complex ecosystem model in a 3-D hydrodynamic model that resolves (sub)mesoscale dynamics remains a challenge [*Lévy et al*., 2012].

## 7. Conclusions

This study offers a new vision of the ecological role of eddies in an upwelling system: in addition to the redistribution of coastal material offshore [*Gruber et al*., 2011], eddies are important sites of locally enhanced production. Our findings show that eddies reduce the coastal production by cross-shore export of material at the regional scale, contributing to local vertical export of material to the deep ocean. However, eddies influence the local production and ecosystem dynamics, offering ecological niches for higher trophic levels. The cyclonic eddy formed in a coastal upwelling system sustained biological production for several months while moving offshore. Enhanced production in the eddy's core shows the local effect of the cyclonic eddy on the planktonic ecosystem, compared to eddy exterior waters. Several mechanisms are associated with the sustained biological production in the eddy core. First, trapping of coastal material enables the eddy to leave the coastal upwelling region with high concentrations of plankton and nutrients. Due to the ability of the eddy to trap material in its core waters, the ecosystem is initially driven mainly by recycling of biological material. As the eddy moves offshore, vertical advection of nitrate from below the euphotic zone balances the loss of particulate material from sinking. This local input of nitrate is the consequence of the uplift of the preexisting dome of the nitracline by Ekman pumping and drives high new production at the base of the euphotic zone, accounting for about 1/3 of the total vertically integrated production. Finally, both eddy trapping and Ekman pumping help to isolate and maintain the ecosystem dynamics in the eddy core, with different balances of new and regenerated production in the surface mixed layer and the subsurface layer.

One might expect to find less separation of the surface and subsurface layers in the real ocean than in our simulations (as suggested by the Chl-*a* model-CalCOFI comparison in Figure 3 for the entire domain); we see at least three reasons to support this expectation. First, episodic fluctuations in atmospheric forcings are expected to occasionally produce mixed layers tens of meters deeper than the climatological average thereby bringing some of the subsurface nutrients and phytoplankton upward. However, several weeks can separate such episodic fluctuations leading to important surface-subsurface decoupling. Finally, we have shown that the biomass of large zooplankton species can be enhanced inside eddies as observed in *Goldthwait and Steinberg* [2008]. The corresponding zooplankton species have been shown to be diel migrants [*Landry et al*., 2008b]. Such behavior is not included in NEMURO, but diel vertical migration tends to reduce the surface/subsurface gradient within the eddy due to (i) higher vertical migration within the upper 150 m that occurs mainly at night [*Goldthwait and Steinberg*, 2008] and/or (ii) an increase in the export flux of matter [*Longhurst et al*., 1990; *Steinberg et al*., 2000, 2002; *Al-Mutairi and Landry*, 2001]. These issues are left to future studies, and require much higher resolution simulations and more sophisticated biogeochemical models than employed here.

**Acknowledgments**

This work was supported by CCE-LTER program. We are thankful to Mark D. Ohman (Scripps Institution of Oceanography, UCSD—mohman@ucsd.edu) and to attendees of the 61st Eastern Pacific Ocean Conference (http://easternpacificoceanconference.org/program_2014.html) for their fruitful comments. We also thank Chris A. Edwards and the anonymous reviewers for comments that improved the manuscript. Chl-*a* used in this study are available from SeaWiFS/MODIS—Sea-viewing Wide Field-of-view Sensor/Moderate Resolution Imaging Spectro-radiometer on the NASA Aqua satellites (http://oceancolor.gsfc.nasa.gov). The data used as boundaries and surface forcing for the model study are available from Comprehensive Ocean-Atmosphere Data Set—COADS (http://iridl.ldeo.columbia.edu/SOURCES/.COADS/), Advanced Very High-Resolution Radiometer—AVHRR (http://noaasis.noaa.gov/NOAASIS/ml/avhrr.html), from Quick Scatterometer—QuikScat (http://www.remss.com/missions/qscat), and Ocean General Circulation Model for the Earth Simulator—OFES (http://www.jamstec.go.jp/esc/research/AtmOcn/product/ofes.html). All the numerical runs were performed with the Caparmor high-performance computer facilities available at Ifremer. Numerical data set that supports this article is available upon request to the authors.

## References

Al-Mutairi, H., and M. Landry (2001), Active export of carbon and nitrogen at Station ALOHA by diel migrant zooplankton, *Deep Sea Res., Part II*, *48*, 2083–2103.

Allen, C., J. Kanda, and E. Laws (1996), New production and photosynthetic rates within and outside a cyclonic mesoscale eddy in the North Pacific subtropical gyre, *Deep Sea Res., Part I*, *43*(6), 917–936.

Almazán-Becerril, A., and E. García-Mendoza (2008), Maximum efficiency of charge separation of photosystem II of the phytoplankton community in the Eastern Tropical North Pacific off Mexico: A nutrient stress diagnostic tool?, *Ciencas Mar.*, *34*(1), 29–43.

Almazán-Becerril, A., D. Rivas, and E. García-Mendoza (2012), The influence of mesoscale physical structures in the phytoplankton taxonomic composition of the subsurface chlorophyll maximum off western Baja California, *Deep Sea Res., Part I*, *70*, 91–102, doi:10.1016/j.dsr.2012.10.002.

Beckenbach, E., and L. Washburn (2004), Low-frequency waves in the Santa Barbara Channel observed by high-frequency radar, *J. Geophys. Res.*, *109*, C02010, doi:10.1029/2003JC001999.

Benitez-Nelson, C. R. et al. (2007), Mesoscale eddies drive increased silica export in the subtropical Pacific Ocean, *Science*, *316*, 1017–1021.

Bibby, T. S., M. Y. Gorbunov, K. W. Wyman, and P. G. Falkowski (2008), Photosynthetic community responses to upwelling in mesoscale eddies in the subtropical North Atlantic and Pacific Oceans, *Deep Sea Res., Part II*, *55*(10–13), 1310–1320, doi:10.1016/j.dsr2.2008.01.014.

Blanke, B., and S. Raynaud (1997), Kinematics of the Pacific equatorial undercurrent: An Eulerian and Lagrangian approach from GCM results, *Oceanogr. J. Phys.*, *27*, 1038–1053.

Blanke, B., M. Arhan, G. Madec, and S. Roche (1999), Warm water paths in the equatorial Atlantic as diagnosed with a general circulation model, *J. Phys. Oceanogr.*, *29*(11), 2753–2768, doi:10.1175/1520-0485(1999)029<2753:WWPITE>2.0.CO;2.

Bleck, R., R. Onken, and J. Woods (1988), A two-dimensional model of mesoscale frontogenesis in the ocean, *Q. J. R. Meteorol. Soc.*, *114*, 347–371.

Brown, S. L., M. R. Landry, K. E. Selph, E. Jin Yang, Y. M. Rii, and R. R. Bidigare (2008), Diatoms in the desert: Plankton community response to a mesoscale eddy in the subtropical North Pacific, *Deep Sea Res., Part II*, *55*(10–13), 1321–1333, doi:10.1016/j.dsr2.2008.02.012.

Brzezinski, M. A., and L. Washburn (2011), Phytoplankton primary productivity in the Santa Barbara Channel: Effects of wind-driven upwelling and mesoscale eddies, *J. Geophys. Res.*, *116*, C12013, doi:10.1029/2011JC007397.

Capet, X., F. Colas, J. C. Mcwilliams, and P. Penven (2008), Eddies in eastern boundary subtropical upwelling systems, in *Ocean Modeling in an Eddying Regime*, edited by M. W. Hecht and H. Hasumi, pp. 131–147, AGU, Washington, D. C.

Carton, X. (2010), Oceanic vortices, in *Fronts, Waves and Vortices in Geophysical Flows*, edited by J.-B. Flor, pp. 61–108, Springer, Berlin Heidelberg.

Carton, J. A., and B. S. Giese (2008), A reanalysis of ocean climate using simple ocean data assimilation (SODA), *Mon. Weather Rev.*, *136*(8), 2999–3017, doi:10.1175/2007MWR1978.1.

Chaigneau, A., G. Eldin, and B. Dewitte (2009), Eddy activity in the four major upwelling systems from satellite altimetry (1992–2007), *Prog. Oceanogr.*, *83*(1–4), 117–123, doi:10.1016/j.pocean.2009.07.012.

Chaigneau, A., M. Le Texier, G. Eldin, C. Grados, and O. Pizarro (2011), Vertical structure of mesoscale eddies in the eastern South Pacific Ocean: A composite analysis from altimetry and Argo profiling floats, *J. Geophys. Res.*, *116*, C11025, doi:10.1029/2011JC007134.

Chavez, F. P., and S. L. Smith (1995), Biological and chemical consequences of open ocean upwelling, in *Upwelling in the Oceans: Modern Processes and Ancient records*, edited by C. P. Summerhayes, et al., pp. 149–169, Environ. Sci. Res. Rep. ES 18, Wiley, N. Y.

Chelton, D. B., M. G. Schlax, and R. M. Samelson (2011a), Global observations of nonlinear mesoscale eddies, *Prog. Oceanogr.*, *91*(2), 167–216, doi:10.1016/j.pocean.2011.01.002..

Chelton, D. B., P. Gaube, M. G. Schlax, J. J. Early, and R. M. Samelson (2011b), The influence of nonlinear mesoscale eddies on near-surface oceanic chlorophyll, *Science*, *334*(6054), 328–32, doi:10.1126/science.1208897.

Chenillat, F., B. Blanke, N. Grima, P. J. S. Franks, and P. Rivière (2015), Quantifying tracer dynamics in a moving fluids: A combined Eulerian-Lagrangian approach, *Front. Environ. Sci. 3*, 43. doi:10.3389/fenvs.2015.00043.

Chenillat, F., P. Riviere, X. Capet, E. Di Lorenzo, and B. Blanke (2012), North Pacific Gyre Oscillation modulates seasonal timing and ecosystem functioning in the California Current upwelling system, *Geophys. Res. Lett.*, *39*, L01606, doi:10.1029/2011GL049966.

Chenillat, F., P. Rivière, X. Capet, P. J. S. Franks, and B. Blanke (2013), California coastal upwelling onset variability: Cross-shore and bottom-up propagation in the planktonic ecosystem, *PLoS One*, *8*(5), e62281, doi:10.1371/journal.pone.0062281.

Cloern, J. E., C. Grenz, and L. Vidergar-Lucas (1995), An empirical model of the phytoplankton chlorophyll: Carbon ratio-the conversion factor between productivity and growth rate, *Limnol. Oceanogr.*, *40*(7), 1313–1321, doi:10.4319/lo.1995.40.7.1313.

Colas, F., J. C. McWilliams, X. Capet, and J. Kurian (2011), Heat balance and eddies in the Peru-Chile current system, *Clim. Dyn.*, *39*(1-2), 509–529, doi:10.1007/s00382-011-1170-6.

Correa-Ramirez, M. (2007), Mesoscale eddies and high chlorophyll concentrations off central Chile (29–39 S), *Geophys. Res. Lett.*, *34*, L12604, doi:10.1029/2007GL029541.

Crawford, W. R. (2005), Heat and fresh water transport by eddies into the Gulf of Alaska, *Deep Sea Res., Part II*, *52*(7-8), 893–908, doi:10.1016/j.dsr2.2005.02.003.

Crawford, W. R., P. J. Brickley, T. D. Peterson, and A. C. Thomas (2005), Impact of Haida eddies on chlorophyll distribution in the Eastern Gulf of Alaska, *Deep Sea Res., Part II*, *52*(7-8), 975–989, doi:10.1016/j.dsr2.2005.02.011.

Dietze, H., R. Matear, and T. Moore (2009), Nutrient supply to anticyclonic meso-scale eddies off western Australia estimated with artificial tracers released in a circulation model, *Deep Sea Res., Part I*, *56*(9), 1440–1448, doi:10.1016/j.dsr.2009.04.012.

Dugdale, R., and J. Goering (1967), Uptake of new and regenerated forms of nitrogen in primary productivity, *Limnol. Oceanogr.*, *12*, 196–206.

Early, J. J., R. M. Samelson, and D. B. Chelton (2011), The evolution and propagation of Quasigeostrophic ocean eddies, *J. Phys. Oceanogr.*, *41*(8), 1535–1555, doi:10.1175/2011JPO4601.1.

Eppley, R., and B. Peterson (1979), Particulate organic matter flux and planktonic new production in the deep ocean, *Nature*, *282*, 677–680.

Falkowski, P., D. Ziemann, Z. Kolber, and P. Bienfang (1991), Role of eddy pumping in enhancing primary production in the ocean, *Nature*, *352*, 55–58.

Feng, M., L. J. Majewski, C. B. Fandry, and A. M. Waite (2007), Characteristics of two counter-rotating eddies in the Leeuwin Current system off the Western Australian coast, *Deep Sea Res., Part II*, *54*(8–10), 961–980, doi:10.1016/j.dsr2.2006.11.022.

Flierl, G. R. (1981), No Particle motions in large-amplitude wave fields, *Geophys. Astrophys. Fluid Dyn.*, *18*(1-2), 39–74, doi:10.1080/03091928108208773.

Franks, P. J. S., J. S. Wroblewski and G. R. Flierl (1986), Prediction of phytoplankton growth in response to the frictional decay of a warm-core ring, *J. Geophys. Res.*, *91*(C6), 7603–7610.

Garcia, H. E., R. A. Locarnini, T. P. Boyer, and J. I. Antonov (2006), World Ocean Atlas 2005, Volume 4: Nutrients (phosphate, nitrate, silicate), edited by S. Levitus, NOAA Atlas NESDIS 64, 396 pp., U.S. Govern. Print. Off., Washington, D. C.

Gaube, P. (2012), Satellite Observations of the Influence of Mesoscale Ocean Eddies on Near-Surface Temperature, *Phytoplankton and Surface Stress*, Oreg. State Univ., Corvallis.

Gent, P. R., and J. C. Mcwilliams (1990), Isopycnal mixing in ocean models, *J. Oceanogr.*, *20*, 150–155, doi:http://dx.doi.org/10.1175/1520-0485(1990)020<0150:IMIOCM>2.0.CO;2.

Goldthwait, S. A., and D. K. Steinberg (2008), Elevated biomass of mesozooplankton and enhanced fecal pellet flux in cyclonic and mode-water eddies in the Sargasso Sea, *Deep Sea Res., Part II*, *55*(10–13), 1360–1377, doi:10.1016/j.dsr2.2008.01.003.

Gower, J., K. Denman, and R. Holyer (1980), Phytoplankton patchiness indicates fluctuation spectrum of mesoscale oceanic structure, *Nature*, *288*, 157–159.

Gruber, N., Z. Lachkar, H. Frenzel, P. Marchesiello, M. Munnich, J. C. McWilliams, T. Nagai, and G.-K. Plattner (2011), Eddy-induced reduction of biological production in eastern boundary upwelling systems, *Nat. Geosci.*, *4*(11), 787–792.

Haury, L. R., J. A. McGowan, and P. H. Wiebe (1978), Patterns and processes in the time-space scales of plankton distributions, in *Spatial Pattern in Plankton Communities*, edited by J. H. Steele, pp. 277–327, Springer, N. Y.

Hayward, T. L., and A. W. Mantyla (1990), Physical, chemical and biological structure of a coastal eddy near Cape Mendocino, *J. Mar. Res.*, *48*, 825–850.

Ivchenko, V. O., Danilov, S., and D. Olbers (2008). Eddies in numerical models of the Southern Ocean, in *Ocean Modeling in an Eddying Regime*, edited by M. W. Hecht and H. Hasumi, pp. 177–198, AGU, Washington, D. C.

Jenkins, W. J. (1988), Nitrate flux into the euphotic zone near Bermuda, *Nature*, *331*, 521–523, doi:10.1038/331521a0.

Kishi, M., M. Kashiwai, D. Ware, B. Megrey, D. Eslinger, F. Werner, M. Noguchiaita, T. Azumaya, M. Fujii, and S. Hashimoto (2007), NEMURO: A lower trophic level model for the North Pacific marine ecosystem, *Ecol. Modell.*, *202*(1–2), 12–25, doi:10.1016/j.ecolmodel.2006.08.021.

Klein, P., and G. Lapeyre (2009), The oceanic vertical pump induced by mesoscale and submesoscale turbulence, *Ann. Rev. Mar. Sci.*, *1*, 351–75, doi:10.1146/annurev.marine.010908.163704.
Kurian, J., F. Colas, X. Capet, J. C. McWilliams, and D. B. Chelton (2011), Eddy properties in the California Current System, *J. Geophys. Res.*, *116*, C08027, doi:10.1029/2010JC006895.
Landry, M. R., S. L. Brown, Y. M. Rii, K. E. Selph, R. R. Bidigare, E. J. Yang, and M. P. Simmons (2008a), Depth-stratified phytoplankton dynamics in Cyclone Opal, a subtropical mesoscale eddy, *Deep Sea Res., Part II*, *55*(10–13), 1348–1359, doi:10.1016/j.dsr2.2008.02.001.
Landry, M. R., M. Decima, M. P. Simmons, C. C. S. Hannides, and E. Daniels (2008b), Mesozooplankton biomass and grazing responses to Cyclone Opal, a subtropical mesoscale eddy, *Deep Sea Res., Part II*, *55*(10-13), 1378–1388, doi:10.1016/j.dsr2.2008.01.005.
Lapeyre, G., and P. Klein (2006), Dynamics of the upper oceanic layers in terms of surface quasigeostrophy theory, *J. Phys. Oceanogr.*, *36*, 165–176.
Lathuilière, C., V. Echevin, M. Lévy, and G. Madec (2010), On the role of the mesoscale circulation on an idealized coastal upwelling ecosystem, *J. Geophys. Res.*, *115*, C09018, doi:10.1029/2009JC005827.
Lee, M. M., D. P., Marshall, and R. G. Williams. (1997). On the eddy transfer of tracers: Advective or diffusive?, *J. Mar. Res.*, (*55*), 483–505.
Lehahn, Y., F. d'Ovidio, M. Lévy, Y. Amitai, and E. Heifetz (2011), Long range transport of a quasi isolated chlorophyll patch by an Agulhas ring, *Geophys. Res. Lett.*, *38*, L16610, doi:10.1029/2011GL048588.
Lévy, M. (2008), The Modulation of Biological Production by Oceanic Mesoscale Turbulence, in *Transport and Mixing in Geophysical Flows, vol. 261*, edited by J. B. Weiss and A. Provenzale, pp. 219–261, Springer, Berlin.
Lévy, M., P. Klein, and A. Treguier (2001), Impact of sub-mesoscale physics on production and subduction of phytoplankton in an oligotrophic regime, *J. Mar. Res.*, *59*, 535–565.
Lévy, M., R. Ferrari, P. J. S. Franks, A. P. Martin, and P. Rivière (2012), Bringing physics to life at the submesoscale, *Geophys. Res. Lett.*, *39*, L14602, doi:10.1029/2012GL052756.
Li, Q. P., P. J. S. Franks, M. R. Landry, R. Goericke, and A. G. Taylor (2010), Modeling phytoplankton growth rates and chlorophyll to carbon ratios in California coastal and pelagic ecosystems, *J. Geophys. Res.*, *115*, G04003, doi:10.1029/2009JG001111.
Longhurst, A. R., A. W. Bedo, W. G. Harrison, E. J. H. Head and D. D. Sameoto (1990). Vertical flux of respiratory carbon by oceanic diel migrant biota, *Deep Sea Res., Part A*, *37*, 685–694.
Mahadevan, A., L. N. Thomas, and A. Tandon (2008), Comment on "Eddy/wind interactions stimulate extraordinary mid-ocean plankton blooms", *Science*, *320*(5875), 448b, doi:10.1126/science.1152111.
Mahaffey, C., C. R. Benitez-Nelson, R. R. Bidigare, Y. Rii, and D. M. Karl (2008), Nitrogen dynamics within a wind-driven eddy, *Deep Sea Res., Part II*, *55*(10–13), 1398–1411, doi:10.1016/j.dsr2.2008.02.004.
Mantyla, A. W., S. J. Bograd, and E. L. Venrick (2008), Patterns and controls of chlorophyll-a and primary productivity cycles in the Southern California Bight, *J. Mar. Syst.*, *73*(1-2), 48–60, doi:10.1016/j.jmarsys.2007.08.001.
Martin, A., and K. Richards (2001), Mechanisms for vertical nutrient transport within a North Atlantic mesoscale eddy, *Deep Sea Res., Part II*, *48*(4-5), 757–773, doi:10.1016/S0967-0645(00)00096-5.
Masumoto, Y. et al. (2004), A fifty-year eddy-resolving simulation of the World Ocean: Preliminary outcomes of OFES (OGCM for the Earth Simulator), *J. Earth Simul.*, *1*(April), 35–56.
McGowan, J. A. (1967), Distributional atlas of pelagic molluscs in the California Current region, *Calif. Coop. Ocean. Fish. Invest.*, *6*, 1–218.
McGillicuddy, D. J., and R. Johnson (1999), Mesoscale variations of biogeochemical properties in the Sargasso Sea, *J. Geophys. Res.*, *104*(C6), 381–394.
McGillicuddy, D. J., and V. Kosnyrev (2001), Covariation of mesoscale ocean color and sea-surface temperature patterns in the Sargasso Sea, *Deep Sea Res., Part II*, *48*(48), 1823–1836.
McGillicuddy, D. J., and A. Robinson (1997), Eddy-induced nutrient supply and new production in the Sargasso Sea, *Deep Sea Res., Part I*, *44*(8), 1427–1450. [CrossRef][10.1016/S0967-0637(97)00024-1].
Mcgillicuddy, D. J., A. R. Robinson, D. A. Siegel, H. W. Jannasch, R. Johnson, T. D. Dickey, J. McNeil, A. F. Michaels, and A. H. Knap (1998), Influence of mesoscale eddies on new production in the Sargasso Sea, *Nature*, *394*, 263–266.
McGillicuddy, D. J. et al. (2007), Eddy/wind interactions stimulate extraordinary mid-ocean plankton blooms, *Science*, *316*(5827), 1021–1026, doi:10.1126/science.1136256.
Moore, T. S., R. J. Matear, J. Marra, and L. Clementson (2007), Phytoplankton variability off the Western Australian Coast: Mesoscale eddies and their role in cross-shelf exchange, *Deep Sea Res., Part II*, *54*(8–10), 943–960, doi:10.1016/j.dsr2.2007.02.006.
Morales, C. E., S. Hormazabal, M. Correa-Ramirez, O. Pizarro, N. Silva, C. Fernandez, V. Anabalón, and M. L. Torreblanca (2012), Mesoscale variability and nutrient–phytoplankton distributions off central-southern Chile during the upwelling season: The influence of mesoscale eddies, *Prog. Oceanogr.*, *104*, 17–29, doi:10.1016/j.pocean.2012.04.015.
Nencioli, F., V. S. Kuwahara, T. D. Dickey, Y. M. Rii, and R. R. Bidigare (2008), Physical dynamics and biological implications of a mesoscale eddy in the lee of Hawai'i: Cyclone Opal observations during E-Flux III, *Deep Sea Res., Part II*, *55*(10–13), 1252–1274, doi:10.1016/j.dsr2.2008.02.003.
Nishimoto, M. M., and L. Washburn (2002), Patterns of coastal eddy circulation and abundance of pelagic juvenile fish in the Santa Barbara, *Mar. Ecol. Prog. Ser.*, *241*, 183–199.
Oschlies, A. (2002), Nutrient supply to the surface waters of the North Atlantic: A model study, *J. Geophys. Res.*, *107*(C5), 3046, doi:0148–0227/02/2000JC000275.
Oschlies, A. (2008), Eddies and upper-ocean nutrient supply, in *Ocean Modeling in an Eddying Regime*, edited by M. W. Hecht and H. Hasumi, pp. 115–130, AGU, Washington, D. C.[WorldCat].
Oschlies, A., and V. Garcon (1998), Eddy-induced enhancement of primary production in a model of the North Atlantic Ocean, *Nature*, *394*(July), 1994–1997.
Owen, R. W. J. (1980), Eddies of the California Current System: Physical and ecological characteristics, in *The California Islands: Proceedings of a Multidisciplanary Symposium*., edited by M. D. Power, pp. 237–263, Santa Barbara Mus. of Nat. Hist., Santa Barbara, Calif.
Penven, P., P. Marchesiello, L. Debreu, and J. Lefèvre (2008), Software tools for pre- and post-processing of oceanic regional simulations, *Environ. Model. Software.*, *23*(5), 660–662, doi:10.1016/j.envsoft.2007.07.004.
Peterson, T., D. Crawford, and P. Harrison (2011), Evolution of the phytoplankton assemblage in a long-lived mesoscale eddy in the eastern Gulf of Alaska, *Mar. Ecol. Prog. Ser.*, *424*, 53–73, doi:10.3354/meps08943.
Rii, Y. M., S. L. Brown, F. Nencioli, V. Kuwahara, T. Dickey, D. M. Karl, and R. R. Bidigare (2008), The transient oasis: Nutrient-phytoplankton dynamics and particle export in Hawaiian lee cyclones, *Deep Sea Res., Part II*, *55*(10–13), 1275–1290, doi:10.1016/j.dsr2.2008.01.013.
Rose, K., B. Megrey, F. Werner, and D. Ware (2007), Calibration of the NEMURO nutrient–phytoplankton–zooplankton food web model to a coastal ecosystem: Evaluation of an automated calibration approach, *Ecol. Modell.*, *202*(1-2), 38–51, doi:10.1016/j.ecolmodel.2006.08.016.

Sangrà, P., J. L. Pelegrí, A. Hernández-Guerra, Igor Arregui, J. M. Martín, A. Marrero-Díaz, A. Martínez, A. W. Ratsimandresy, and A. Rodríguez-Santana (2005), Life history of an anticyclonic eddy, *J. Geophys. Res.*, *110*, C03021, doi:10.1029/2004JC002526.

Sangrà, P. et al. (2009), The Canary Eddy Corridor: A major pathway for long-lived eddies in the subtropical North Atlantic, *Deep Sea Res., Part I*, *56*(12), 2100–2114, doi:10.1016/j.dsr.2009.08.008.

Sasaki, H., Y. Sasai, M. Kawahara, F. Furuichi, A. Araki, A. Ishida, Y. Yamanaka, Y. Masumoto, and H. Sakuma (2004), A series of eddy-resolving ocean simulations in the world ocean: OFES (OGCM for the Earth Simulator) project, in *OCEAN'04*, MTTS/IEEE TECHNO-OCEAN'04, vol. 3, pp. 1535–1541, IEEE.

Sasaki, H., M. Nonaka, Y. Masumoto, Y. Sasai, H. Uehara, and H. Sakuma (2006), An eddy -resolving hindcast simulation of the quasi-global ocean from 1950 to 2003 on the Earth Simulator, in *High Resolution Numerical Modelling of the Atmosphere and Ocean*, edited by W. Ohfuchi and K. Hamilton, Springer, N. Y.

Shchepetkin, A. F., and J. C. McWilliams (2005), The regional oceanic modeling system (ROMS): A split-explicit, free-surface, topography-following-coordinate oceanic model, *Ocean Modell.*, *9*(4), 347–404, doi:10.1016/j.ocemod.2004.08.002.

Siegel, D. A., D. J. McGillicuddy Jr., and E. A. Fields (1999), Mesoscale eddies, satellite altimetry, and new production in the Sargasso Sea, *J. Geophys. Res.*, *104*(C6), 359–380.

Siegel, D. A., P. Peterson, D. J. McGillicuddy, S. Maritorena, and N. B. Nelson (2011), Bio-optical footprints created by mesoscale eddies in the Sargasso Sea, *Geophys. Res. Lett.*, *38*, L13608, doi:10.1029/2011GL047660.

Steinberg, D. K., C. A. Carlson, N. R. Bates, S. A. Goldthwait, L. P. Madin, and A. F. Michaels (2000), Zooplankton vertical migration and the active transport of dissolved organic and inorganic carbon in the Sargasso Sea, *Deep Sea Res., Part I*, *47*, 137–158.

Steinberg, D. K., S. A. Goldthwait, and D. A. Hansell (2002), Zooplankton vertical migration and the active transport of dissolved organic and inorganic nitrogen in the Sargasso Sea, *Deep Sea Res., Part I*, *49*, 1445–1461.

Stern, M. E. (1965), Interaction of a uniform wind stress with a geostrophic vortex, *Deep Sea Res. Oceanogr. Abstr.*, *12*, 355–367.

Stramma, L., H. W. Bange, R. Czeschel, A. Lorenzo, and M. Frank (2013), On the role of mesoscale eddies for the biological productivity and biogeochemistry in the eastern tropical Pacific Ocean off Peru, *Biogeosciences*, *10*, 7293–7306, doi:10.5194/bg-10-7293-2013.

Strass, V. H. (1992), Chlorophyll patchiness caused by mesoscale upwelling at fronts, *Deep Sea Res., Part A*, *39*(1), 75–96, doi:10.1016/0198-0149(92)90021-K.

Suggett, D., C. Moore, A. Hickman, and R. Geider (2009), Interpretation of fast repetition rate (FRR) fluorescence: Signatures of phytoplankton community structure versus physiological state, *Mar. Ecol. Prog. Ser.*, *376*, 1–19, doi:10.3354/meps07830.

Sweeney, E. N., D. J. McGillicuddy, and K. O. Buesseler (2003), Biogeochemical impacts due to mesoscale eddy activity in the Sargasso Sea as measured at the Bermuda Atlantic Time-series Study (BATS), *Deep Sea Res., Part II*, *50*(22–26), 3017–3039, doi:10.1016/j.dsr2.2003.07.008.

The Ring Group (1981), Gulf Stream Cold-Core Rings: Their Physics, Chemistry, and Biology, *Science*, *212*(4499), 1091–1100.

Thomas, C. (1999), Seasonal distributions of satellite-measured phytoplankton pigment concentration along the Chilean coast, *J. Geophys. Res.*, *104*(C11), 877–890.

Thomas, L. N. (2005), Destruction of potential vorticity by winds, *J. Phys. Oceanogr.*, *35*(1994), 2457–2466.

Thomas, L. N., and P. B. Rhines (2002), Nonlinear stratified spin-up, *J. Fluid Mech.*, *473*, 211–244, doi:10.1017/S0022112002002367.

Wainwright, T. C., L. R. Feinberg, R. C. Hooff, and W. T. Peterson (2003), A comparison of two lower trophic models for the California Current System, *Ecol. Modell.*, *202*, 120–131, doi:10.1029/2001JC001182.

Woods, J. (1988), Scale upwelling and primary production, in *Toward a Theory on Biological-Physical Interactions in the World Ocean*, edited by B. J. Rothschild, pp. 7–38, Springer, Netherlands..

Yentsch, C. S., and D. A. Phinney (1985), Rotary motions and convection as a means of regulating primary production in warm core rings, *J. Geophys. Res.*, *90*(C2), 3237–3248.